DESIGN AND DEVELOPMENT BIDIRECTIONAL INTEGRATED CONVERTER FOR PLUG-IN ELECTRIC VEHICLES

A Dissertation submitted in fulfillment of the requirements for the Degree of

MASTER OF ENGINEERING

In

Power Systems

Submitted By

Harsh Ratan Guleria

(Roll No.802042007)

Under the guidance of

Dr. Anjanee Kumar Mishra

Assistant Professor, EIED

2022

Electrical and Instrumentation Engineering Department
Thapar Institute of Engineering & Technology, Patiala
(Declared as Deemed-to-be-University u/s 3 of the UGC Act., 1956)
Post Bag No. 32, Patiala – 147004

DECLARATION CERTIFICATE

I hereby certify that the work which is being presented in the dissertation entitled **"Design and Development of Bidirectional Integrated Converter for Plug-in Electric Vehicles"** in partial fulfillment of the requirement for the award of the degree of Master of Engineering in Power Systems, submitted in the Electrical and Instrumentation Engineering Department of Thapar Institute of Engineering and Technology, Patiala has been carried out under the guidance of **Dr. Anjanee Kumar Mishra**, Assistant Professor, EIED. This work is a representation of the ideas in my own words and where others' ideas or words have been included, I have adequately cited and referenced the original source.

Place: Patiala
Date: 19-07-2022

Harsh Ratan Guleria
(Rollno.:80204207)

It is certified that the above statement made by the student is correct to the best of my knowledge & belief.

Place: Patiala
Date: 19-07-2022

Dr.Anjanee Kumar Mishra
Assistant Professor
Electrical and Instrumentation Engineering Department
Thapar Institute of Engineering and Technology, Patiala

ACKNOWLEDGEMENT

I would like to thank the Thapar Institute of Engineering and Technology, Patiala for giving me the opportunity to use its resources & work in an inspiring atmosphere.

First and foremost, I take this opportunity to express my deepest sense of gratitude to my guide **Dr. Anjanee Kumar Mishra,** Assistant Professor, Thapar Institute of Engineering and Technology, Patiala for his able guidance during my dissertation work. This dissertation would not have been possible without his help and the valuable time given him amidst his busy schedule. I would like to express my deepest sense of gratitude towards **Dr. R.S. Kaler** Senior Professor, and Head, EIED has been a constant source of inspiration for me throughout the preparation.

I would also like to extend my gratitude to my parents and friends of this department who have always encouraged and supported the information this work

Last but one least I would like to thank all the staff members of the **Department of Electrical and Instrumentation Engineering** who have been very cooperative with me.

Harsh Ratan Guleria

(Roll no.:802042007)

TABLE OF CONTENTS

LIST OF FIGURES

LIST OF TABLE

LIST OF NOMENCLATURE

EV	Electric vehicle
BEV	Battery electric vehicle
HEV	Hybrid electric vehicle
FCEV	Fuel Cell Electric Vehicle
PHEV	Plug-In Hybrid Electric Vehicle
ICE	Internal Combustion Engine
PFC	Power Factor Correction
SAE	Society Of Automotive Engineers
DBR	Diode Bridge Rectifier
THD	Total Harmonics Distortion
CCM	Continuous-Conduction Mode
DCM	Discontinuous-Conduction Mode
CCS	Combined Charging System
EV-PV	Electric Vehicle-Photovoltaic
MPPT	Maximum Power Point Tracking
PWM	Pulse Width Modulation
MOSFET	Metal-Oxide-Semiconductor Field- Effect Transistor
OLTC	On-Load Tap Changing
SEPIC	Single-Ended Primary-Inductor Converter
VSI	Voltage Source Inverter
PHEV	Plug-In Hybrid Electric Vehicle
LED	Light Emitting Diode
NLC	Nearest Level Control

SOC	State Of Charging
BLDC	Brushless DC Motor
ZCS	Zero Current Switching
VM	Voltage Mode
CPM	Current Programmed Mode
DSP	Digital Signal Processor
BOIB	Boost-Interleaved Buck-Boost
BCM	Boundary Conduction-Mode
PQ	Power Quality
NLCC	Nonlinear Carrier Control
PCC	Point Of Common Coupling
UPF	Unity Power Factor
SPV	Solar Photovoltaic
PEV	Plug-in electric vehicle
PR	Propulsion
RB	Regenerative braking

ABSTRACT

This thesis focuses on the evolution, analysis, and design of improved single-stage based integrated converters aimed at on-board applications of plug-in electric vehicles (achieving complete types of vehicle operation, i.e., plug-in charging, propulsion, and regenerative braking using a single-converter) (PEVs). For better gasoline compromising with health is a big concern to deal with these issues of health due to environmental impacts gasoline may be replaced with EV Collectively known as plug-in electric vehicles (PEVs). In the vehicle's engine has an additional battery charging system, usually between the battery and the traction motor inverter. A bidirectional DC-DC converter is used. This converter is charged with increasing battery voltage and efficiently controlling power during cruising, acceleration, and regenerative braking. The bidirectional DC-DC converter is only employed in propulsion or regenerative modes in such classic designs, and the battery is charged by yet another AC/DC converter. This includes different converters for two independent operating modes, regardless of the converter configurations. Merging the additional mount entity with the bidirectional DC-DC converter, which is used during touring and stepping up modes, would be a competent alternative for providing a highly compact, lightweight, and affordable charging scheme. Both AC-DC and bidirectional converters are used in this notion.

This study proposes a novel integrated converter-based charging system for EVs. To function efficiently and achieve all of its operating modes, the created system only requires a limited number of power electronics components. In the typical system, the bidirectional DC-DC converter is integrated into the on-board resulting in a single converter for the whole operation of PEVs. When compared to an existing integrated converter, the major improvement of this integrated converter is an completely effective progress in propulsion as boost mode and regenerative as buck mode technique.

CHAPTER 1

INTRODUCTION

1.1 Background and Motivation

Land transport sector mainly depends on oil products. Quite a few actions have been reserved in directives to mitigate this craving. On a single indicator, public transport has been developed as rechargeable trains (trams, subway, and high-speed trains). On other indicators, the productivity of private transport has been improved via plummeting the heft of vehicles by using more efficient internal combustion engines (ICEs). However, the enlargements in the ICEs technology are not an adequate amount to significantly shrink lubricant feasting. In this bearing, researchers and carmakers have been working on several options including automobiles that run on biodiesel, ethanol, compressed air, liquefied natural gas (LNG), hydrogen, flattened natural gas (CNG), and electric vehicles (EVs), among other fuels.

Recent developments have led to the penetration of EVs into market as an alternative to conventional vehicles employing ICEs. Enabling policy of developed as well as developing countries and the ever-growing need to curb air pollution in cities has the created most suitable environment for these developments. A number of nations have established emanation ethics that are premeditated to frontier the noxious waste emanations of upcoming vehicles sold in the countries. Furthermore, growing research in battery technology provides improved and more affordable batteries for upcoming EVs; hence, the inclusive charge of EVs is sinking fast. It is expected that sales of EVs will grow continuously for two main reasons: economy of scale and new developments in battery technology. As for the economy of scale, some companies have established battery manufacturing facilities on their own to amend their expenses. Moreover, it must be noted that batteries are being widely used in distributed generation, unmanned vehicle aviation applications, etc., and their cost is bound to fall rapidly.

Supreme EVs are thrilling over and done with a direct connection flanked by vehicle and low voltage distribution network These EVs are plug-in electric cars since they are linked to the grid (PEVs). PEVs may be broken down into three different categories: fuel cell plug-in hybrid electric cars, battery electric vehicles, and plug-in hybrid electric vehicles (PHEV). On the other hand,

hybrid electric cars (HEVs) are not regarded as plug-in electric vehicles (PEVs). Since these cars have ICEs that produce their own power, they do not require a grid to charge their batteries.

The PEVs are nowadays a hopeful clarification to curtail the air fumes that generates clean energy for the car using pollution-free battery power. PEVs combine a battery, an add-on charger, and an inverter-drive system. Battery acting a grave role in the fruition of PEVs. The battery's age and charging cycle have a strong bearing on the traits of battery-powered stallions. The battery chargers for on-board applications have to be small and light since it is placed into vehicles. Therefore, in this direction researchers across the world are working to develop and design of compact charging system for PEVs.

1.2 Objectives of the Thesis

Based on above-mentioned research gaps, the principle objective of this thesis is to develop improved integrated converter for on-board applications of PEVs with focus on one or more of the following points: reduction of active and passive components, improvement of operational efficiency, reduction of feedback element and buck/boost operations in each mode.

To accomplish this, the following research objectives have been formulated:

- The development topology has been analysed for detailed operation, loss analysis, stress (voltage/current) analysis of switching devices and passive components design.
- Creation of computer simulation for proposed topology using MATLAB/Simulink software. Detailed simulation results are presented to verify the suitability of the converter for charging, propulsion and regenerative braking modes.
- Comparative analysis of the proposed integrated converters is carried out with existing integrated converters in terms of efficiency, number of components and buck/boost capabilities for each mode.

1.3 Organization of the Thesis

The content of this thesis is presented in the following chapters

Chapter-I: This chapter introduces a generalized view of electric vehicle and power electronic interferences for charging system. A generalized and detailed state of art highlights the shortcomings in the existing technologies and thereby discloses the scope of the work. Various

technological solutions are introduced, which are identified as the objectives of the work. Finally, an outline of the chapters describes the contents of various chapters of the thesis.

Chapter-II: This chapter deals with a literature survey in the concerned research area. A hierarchy of the development of EV single-stage chargers is discussed. A detailed review and comparative analysis of the various existing EV single-stage is also done. In addition, the stepwise advancement of solar photovoltaic technology and various MPPT techniques are carried out in this chapter.

Chapter-III: This chapter deals with a comparison to current integrated converters, the new integrated converter described in this chapter has improved efficiency in the propulsion boost and regenerative braking modes. The increased efficiency in these two modes allows the car to go farther between charges. Moreover, this converter has low stresses in each mode.

Chapter-IV: In this chapter, the main conclusions and the key achievements of this research work are presented in brief. It also enlists the scope of further work in an EV single stage charging system using multi-objective integrated converters.

CHAPTER 2

LITERATURE REVIEW

This Section focuses on the classification of battery chargers, and literature review of single-stage based chargers for on-board applications. The single-stage chargers are classified into conventional and integrated chargers. These chargers generally employ non-isolated converters which are suitable for compact charging system for on-board charger (OBC).

2.1 Classification of Chargers

PEVs typically have There are two different kinds of battery chargers used: standalone (off-plank) and OBC. The off-batten charging mechanism is employed when a lot of electricity has to be charged. With an off-batten charger, the charger's size and weight are easier to manoeuvre. The OBC is more prevalent because it is placed inside the vehicle; car can thus be recharged everywhere [1 2]. The desired features of OBC are bright heaviness, maximum power density and maximum efficiency [3-7]. The OBC may have two-stage converter (Fig. 2.1) or single-stage converter (Fig. 2.2), at two-stage chargers have large number of components [3, 8-12], the single-stage chargers [13–17] are added striking for on-board bids, even though it suffers from low frequency battery current ripple.

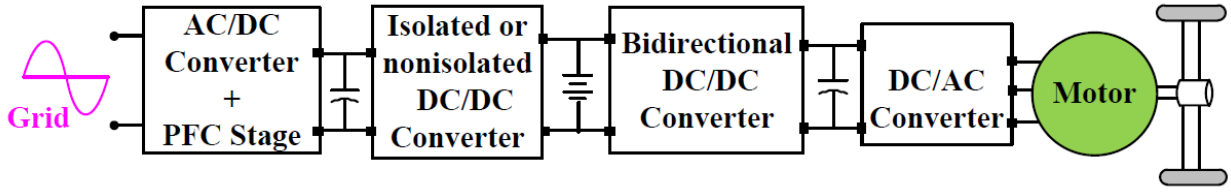

Figure.2.1. Block diagram of the conventional two-stage EV battery charger.

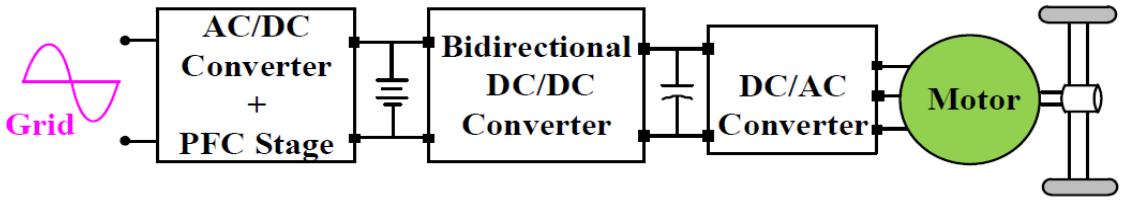

Figure 2.2. Block diagram of single-stage EV battery charger

The vehicle adds in on board charger due to heaviness, capacity, and price tag; therefore, usually, it is designed for power levels (1-2.5 kW) [18, 19]. However, a two-stage converter using

transformer as an isolation is a common rule in OBC design. Galvanic isolation has a negative impact on efficiency and power density due to varied range of output voltage and higher frequency of transformer are there [20–22]. As such, there is no necessity of seclusion for the well-being of EVs as per SAE (Society of Automotive Engineers) J1772 [18]. There is no electrical restraint, or isolation required between battery packs and ac inputs because it the vehicle's ground is floating with the body [18]. Nonetheless, at the output side, battery is added a relay protective circuit due to some safety issues.

2.2 Integrated Chargers with Bidirectional Capability

A traditional single-stage charger is formed from a systematic block diagram of this sort of integrated charger, which is depicted in Fig. 2.3. A bidirectional dc/ac converter connects the battery with dc/dc converter [18] is combined with PFC stage [4, 23] only one converter is required for complete operational modes.

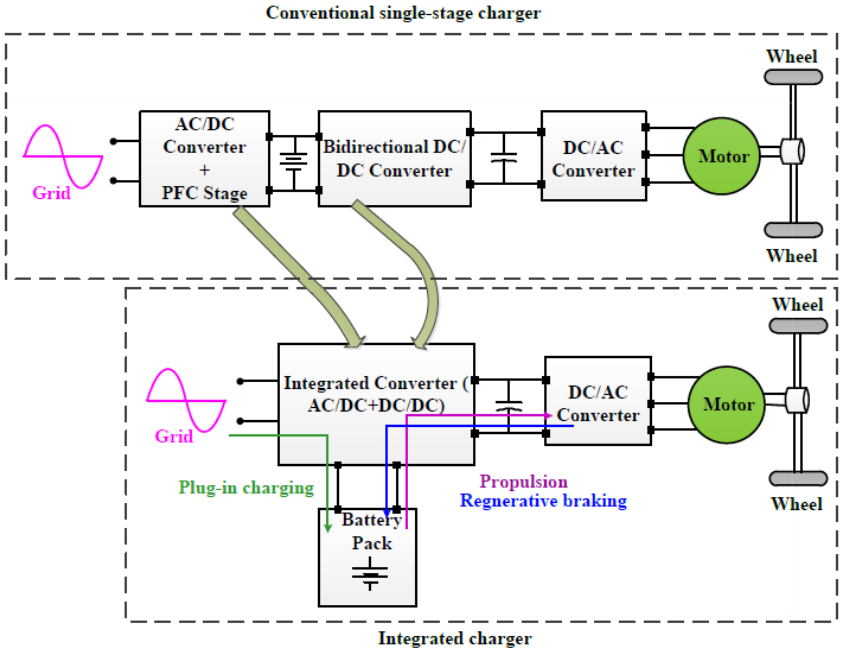

Figure 2.3. Block diagram of an integrated charger utilizing dc/dc converter into the charging circuit.

Because so many components, including diodes, switches, and certain passive parts, are shared throughout the modes, the overall number of machinery is lower than with typical single-stage chargers. Various kinds of these chargers are documented in [17], and all are examined. It is expected that the car is not driven throughout the charging process and that, other than during regeneration braking, the battery pack cannot be charged while the vehicle is being driven.

An integrated charger was proposed in [24], as shown in Fig. 2.4, for all modes of a vehicle with buck/boost operation in each mode. The regenerative braking energy of the buck/boost operations of the converter permitted springy control and proficiency of efficiency are taking.

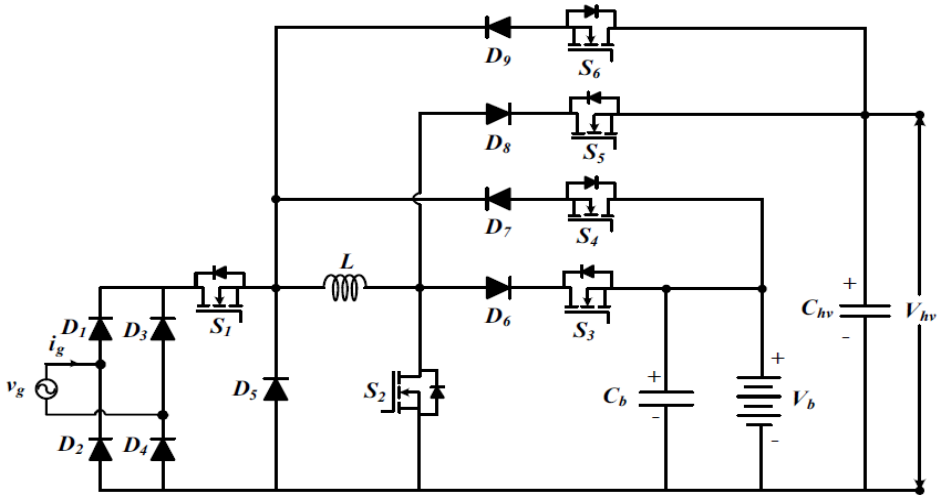

Figure 2.4. Integrated charger [24]

In that type of converter are two to four semiconductor devices are global grid voltage may be used to charge batteries with voltages ranging from 200 to 450 V. in the current track which intensifications conduction losses and shrinks efficacy.

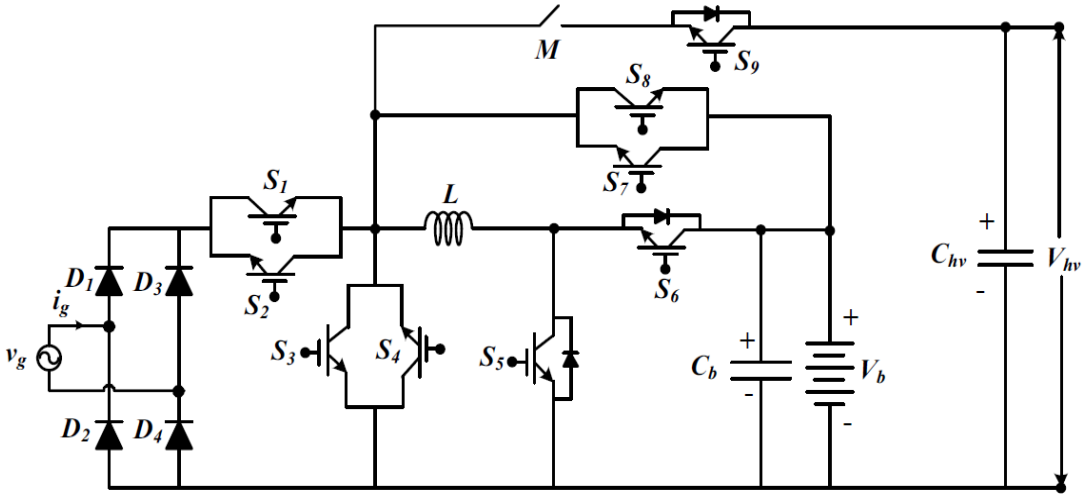

Figure 2.5. Integrated charger [25]

Novelists in [25] have shown a nine-switch integrated charger (Fig. 2.5) that is compatible with any battery voltage altitude. Due to its bridgeless nature in plug-in charging mode, the converter avoids the heat management issues associated with bridge rectifiers and the resulting losses. However, the excessive amount of switches makes OBC applications less desirable. Additionally, a variety of control strategies in this converter call for the activation of co-packed IGBT switches.

An integrated charger technique has been presented in this study [26], as shown in Fig. 2.6 one power drive switch and an inductor is common for all operation, and buck-boost converter play a role of charging/discharging as well as recharging.

The inverting buck/boost and buck and boost operating converter are in charging, recharging, and discharging, following modes are their plug-in, regenerative, propulsion modes respectively.

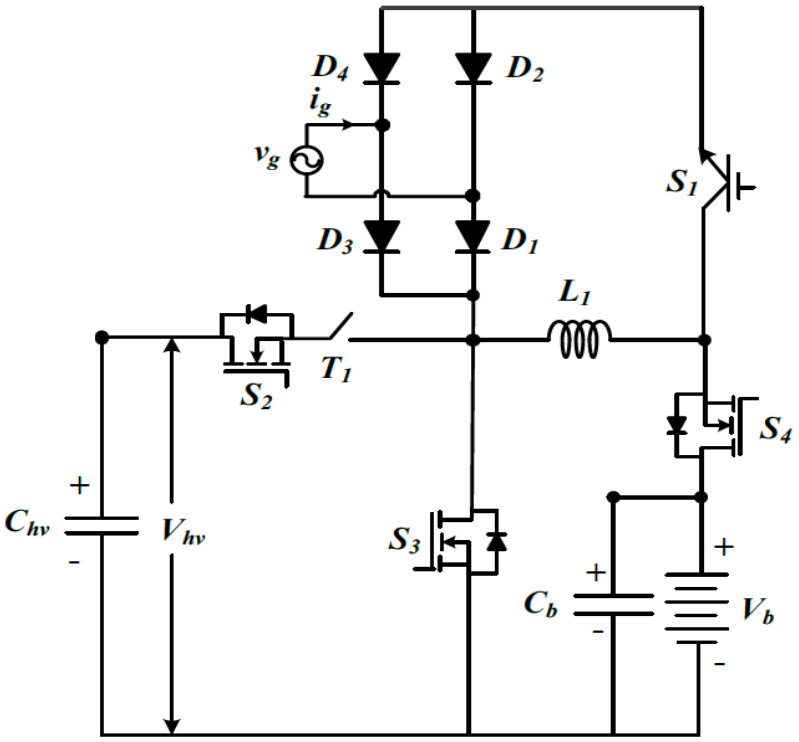

Figure 2.6. Integrated charger [26]

In addition, this converter appearances enhancement above converter [24] based on the quantity of components and effectiveness in each mode. As a result, it provides creators with a cheap elucidation. Nevertheless, the foremost drawbacks of this converter are increased voltage and current stresses in semiconductors and increased current stress in magnetic components. Moreover, Associated with a mechanical switch, the two-switch buck/boost converter in propulsion and regenerative braking modes has more conduction loss than its conventional version.

[27] have proposed an integrated charger, as shown in Fig. 2.7 using four switches and one inductor with sundry semiconductor devices depending on model) in the foremost current lane. Likewise, the per capita technique has comparable switching and conduction losses to its traditional equivalents (buck/boost converters with a single switch or two switches).

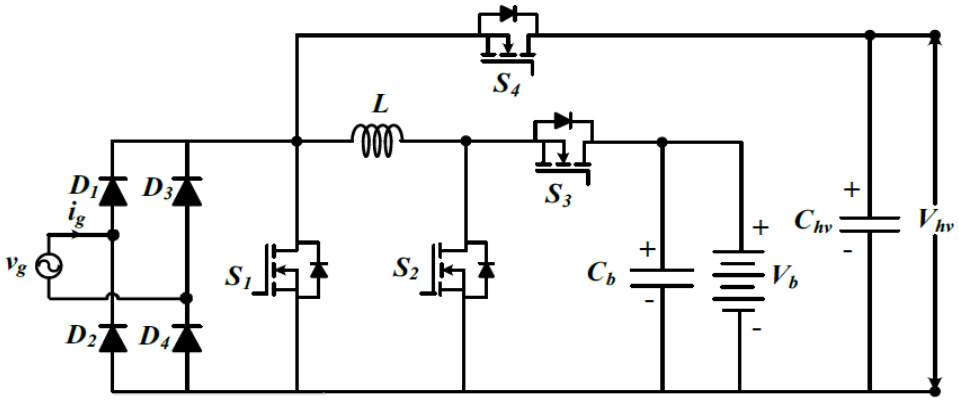

Figure 2.7. Integrated charger [27]

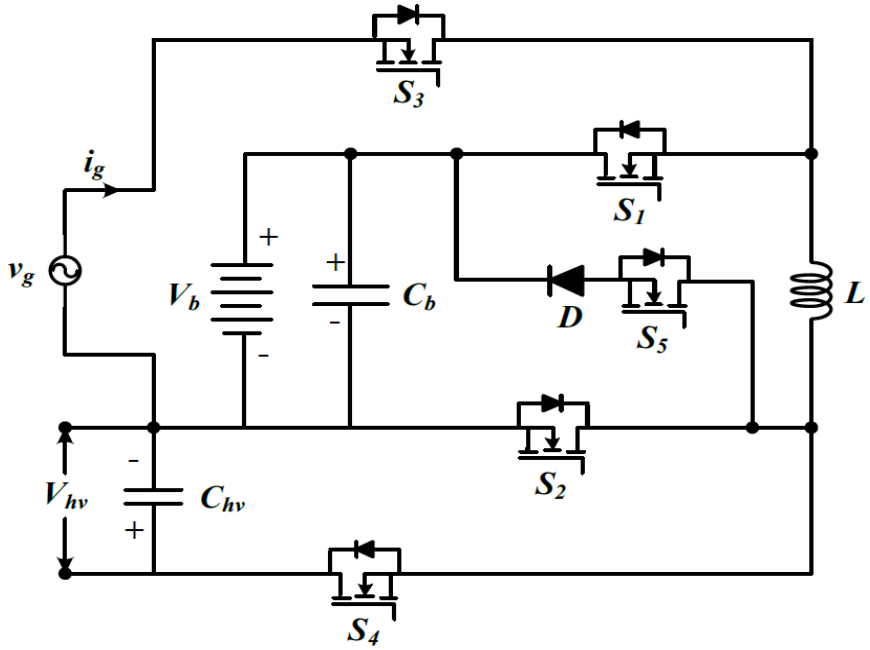

Figure 2.8. Integrated charger [28]

Moreover, Due to the sheer low voltage/current tensions in this converter, there are fewer losses and a slighter rise in temperature, which ultimately slims down the charger. Additionally, by assessing the inductor current, only one current transducer is required for each mode, resulting in a reduced overall design and minimal feedback circuitry. In arrears to boost operation during charging; it is not possible to custody the battery-operated when peak grid voltage becomes o'er battery voltage.

Novelists have proposed a charge non-linear carrier control based bridgeless integrated charger in [28], as shown in Fig. 2.8. The plug-in charging technique has been used with the charge non-linear control based controller (CCM) and is compatible to PFC in continuous conduction mode.

As a result, the charger becomes more compact as the feedback circuity is reduced. The converter's bridgeless design tends to increase converter efficiency in plug-in charging mode by lowering the number of devices in the current route. The converter, however, serves as a typical inverting buck/boost. in a grid's negative half cycle, placing significant pressures rising loses and the ingredients (conduction and switching losses).As a result, during the grid's negative half cycle, the benefit of bridgeless nature is somewhat sacrificed. Moreover the battery's voltage range is constrained since none of the operational modes has both buck and boost abilities [29]. The battery's voltage range is constrained since none of the operational modes has both buck and boost capabilities. For a wide range of battery voltages, as illustrated in Fig.2.9, a quasi two-stage charger has been developed. The proposed converter acts as a typical boost converter (single-stage operation) when the battery voltage V_b > the peak grid voltage V_g;max, and as a quasi two stage converter (two-stage mode) when V_b ,V_g; max. Additionally, two-stage operation is less efficient.. Due to the conduction of an extra switch, this converter has somewhat larger conduction losses in plug-in charging mode than a standard boost PFC converter. Nevertheless, due to the peculiarities of its three-level output voltage, this converter has fewer switching losses. Additionally, the suggested converter functions in boost and buck modes in propulsion and regenerative braking modes, respectively.

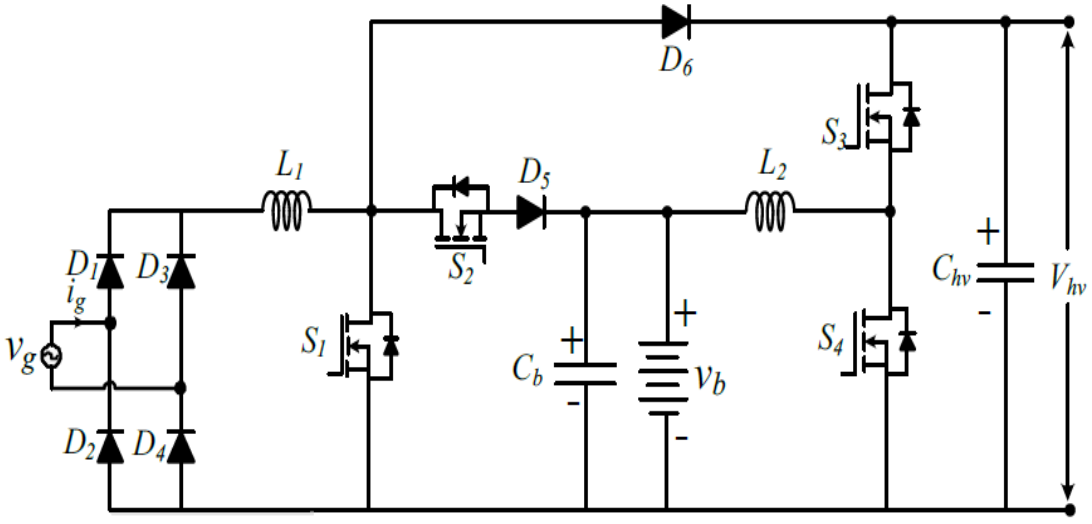

Figure 2.9. Integrated charger [29]

2.3 Comparison of Integrated Chargers

In this Portion,a comparative of integrated chargers have been made based on the voltage/current pressures on semiconductor devices, the buck/boost working of the converter in

each mode, and the total component count. The pressures on semiconductor devices are listed for each mode in Table 2.1., with "High" standing for the total of input and output quantities *(V_{out} + V_{in} and I_{out} + I_{in})* and "Low" standing for either the input or output quantities (V_{out} V_{in})and *(I_{out} or I_{in}).* The integrated charger [95] has both buck/boost operation as indicated in Tables 2.1 and 2.2, and low stresses in each mode, albeit at the consequence of a large number of semiconductor devices.

Table 2.1.

Voltage and Current Stresses in Semiconductors in Each Mode.

Integrated Chargers	Plug-in charging		Propulsion		Regenerative Braking	
	Voltage	Current	Voltage	Current	Voltage	Current
Fig .2.4	Low	Low	Low	Low	Low	Low
Fig .2.5	Low	Low	Low	Low	Low	Low
Fig .2.6	High	High	Low	Low	Low	Low
Fig .2.7	Low	Low	Low	Low	Low	Low
Fig .2.8	High	High	Low	Low	Low	Low
Fig .2.9	Low	Low	Low	Low	Low	Low

Table 2.2.

Comparative Study of the Integrated Chargers in Terms of Buck/Boost Capabilities of Each Mode and Number of Components.

Integrated Chargers	Mode of Operation			Number of Components			
	Plug-in Charging	Propulsion	Regenerative Braking	Switch	Diode	Inductor	Capacitor
Fig .2.4	Buck/boost	Buck/boost	Buck/boost	6	9	1	2
Fig .2.5	Buck/boost	Buck/boost	Buck/boost	9	4	1	2
Fig .2.6	Buck/boost	Boost	Buck	5	5	1	2
Fig .2.7	Boost	Buck/boost	Buck/boost	4	4	1	2
Fig .2.8	Boost or Buck/boost	Boost	Buck	5	1	1	2
Fig .2.9	Boost	Buck/boost	Buck/boost	4	6	2	2

The converter [96] has an efficiency improvement over converter [95] by cutting devices in the current route, but the price of the charger rises since there are more switches. In terms of component count, the charger [97] outperforms the chargers [95,96]. With just boost charging capabilities, the charger [98] has fewer components than any other converter now in use and experiences lower pressures in each mode That charger is[100] operates in buck/boost mode while

being in plug-in charging mode, although this mode necessitates a sophisticated control technique. Moreover, the two-stage operation of the converter during buck mode sacrifices its advantages.

From the above literature review, it is evident that there is a scope of further improvement in integrated converters by developing converters with feature buck/boost capabilities in each mode, minimise the amount of components, and enhance propulsion and regenerative braking efficiency to enable longer running times. In addition to this, reduction of complexity of feedback circuit will reduce size of the converter and improves reliability of the converter.

2.4 History And Development of Solar PV Array Technology

The history of solar technology from the 7th century B.C. until the present. It has started using mirrors and glass to focus the sun's heat in order to spark fires. These days, this technique is used in both solar-powered cars and structures. The turning points in the history of solar technology, year by year and from the 7th century B.C. to the present. Photovoltaic technology actually dates back over 177 years Alexandre Edmond Becquerel, a 19-year-old French scientist, discovered a physical phenomena that allowed light to be converted into electricity in 1839 while experimenting with metal electrodes and electrolyte. Although the fundamentals of science were originally discovered in 1839, development truly took off in the 20th century [30–36]. A substantial advancement in solar PV technology has led to a rapid increase in PV installation around the globe. At least 227.1 GW of installed capacity was available globally as of the end of 2015 [37]. With 43.5 GW, China now has the highest cumulative capacity, followed by Germany with 39.7 GW, Japan with 34.4 GW, the USA with 25.6 GW, and Italy with 18.9 GW [38-39].. As of the end of August 2016, the Indian government's Ministry of New & Renewable Energy (MNRE) has installed a total of 8.4 GW of PV arrays. [40].

A high diminishing rate of the cost of PV array generation further attracts an electricity consumer for such diverse applications as residential, agriculture, health, industry, telecommunication, transportations, and public services. The PV technology possesses a delightful economic development history. A viable photovoltaic maneuver with a 2 percent efficiency costing $25 per cell and a 14 MW peak output was first offered by Hoffman Electronics-Semiconductor Division in 1955. The energy cost has been US$ 1,785 per watt [41]. A successive development has led to a drastic reduction in the cost as low as US$ 30 per watt, 18 years later, in 1973. Today, the technology has reached a milestone as the price of a high-efficiency Multi-Si Cell and Mono-Si

cell has dropped to US$ 0.18 per watt [42]. In addition, there has been a tremendous improvement in the efficiency of a solar cell since 1941. The first silicon monocrystalline solar cell has been constructed in 1941 and has less than 1% conversion efficiency [42]. Within a time, span of 75 years, today the global market is full of 44.7% efficiency solar cells. These have been possible due to the advancement in material science, enriching the PV technology in terms of economy, efficiency, performance, and durability.

2.5 Standards, Testing And Quality Certification For Solar PVArray Systems

For this technology to be successfully implemented on a large scale, quality certification and pertinent standards for solar PV system design and installation are crucial. Additionally, it is crucial to establish a strict and effective monitoring system to ensure compliance with these criteria [43] For the benefit of solar panel producers, exporters, installers, and suppliers, this section offers details on standards, certification programmers, and other industry-specific information. On the proposal of the Solar Photovoltaic Energy Systems Sectional Committee and with the consent of the Electro technical Division Council, the Bureau of Indian Standards (BIS) has approved a number of IEC standards (IEC) [44-47], e.g. *IEC/TS 62548*: *2013* for PV array design requirements and *IEC 62109 - 1, 2* for the safety of power converters. References to several international standards for which Indian standards also exist can be found in these accepted standards. For PV modules and converters, the applicable Indian standards, which are to be substituted in their places, along with the other adopted standards, are listed in Table 2.1. The current compliance regime applying to solar PV generation is overseen by a number of regulatory bodies including Clean Energy Council (CEC) [48], Clean Energy Regulator (CER) [76], Standards Australia [48], European Standard [49-52], and Californian standard [52], etc

2.6 Review of MPPT Techniques for Solar PV Array Generation

The PV array offers a nonlinear V-I characteristic across its terminals. The same PV array delivers different power outputs at different operating points. Therefore, in order to utilize the PV array to its full capacity, the PV arrays are operated near to MPP point. Since the MPP point changes with change in ambiance conditions (temperature and insolation), various MPPT algorithms are proposed by several researchers. These MPPT algorithms provide reference signals to control the associated power converter, such that the impedance across PV array terminals is so

Table 2.3

Standards, Testing and Quality Requirements for Solar PV Systems

International Standard	Corresponding Indian Standard	Description
IEC 61215	IS 14286	Intention condition and type consent for crystalline silicon terrestrial PV modules
IEC 61646	IS 16077	Enterprise requirement and type consent for thin-film telluric PV modules
IEC 61853-Part 1	IS 16170: Part 1	PV building block concert trying and energy sailor: Irradiance and temperature recital extents, and power rating
IEC 60904-1	IS 12762: Part 1	PV systems: Assessment of PV current and voltage manifestations, Part 1
IEC 61730-1, 2	IS 61730-1, 2	PV building block well-being condition – Part 1: Necessities for construction, Part 2: Desires for testing
ISO/IEC 17025	IS 17025	Broad standards for the competency of testing and tuning laboratories
IEC 60364-7-712	SP 30	Necessities for distinct fixings or scenes – Solar PV array power supply coordination
IEC 61701	-	Briny haze rust taxing of PV building block
IEC 62716	-	PV building block – Ammonia (NH3) corrosion taxing
IEC 62804	-	PV building block - Test ways and means for the detection of potential-induced degradation (PID). IEC TS 62804- 1: Part 1: Crystalline silicon
IEC 62759-1	-	PV building block – Transportation testing, Part 1: Transportation and shipping of section package units

adjusted that it operates near to MPP. A review and comparison of various MPPT algorithms are reported in [49]-[61].

The MPPT techniques can be broadly divided into two groups: conventional techniques like perturbation and observation (P&O) [62–66] and incremental conductance (InC) [63–64] and intelligent techniques like fuzzy logic (FL) [67–71] and MPPT techniques based on artificial neural networks (ANN) [72–73]. Although intelligent approaches are quicker and more effective than traditional ones, which are often easy, inexpensive, and less effective, they are more sophisticated. The MPPT techniques can also be divided into direct and indirect techniques. The indirect approaches, including open-circuit and short-circuit methods [74], depend on mathematical

relationships that may not account for all climatic situations or call for previous knowledge of the PV array's properties. As a result, They are still unable to accurately track the MPP of the PV array at any irradiance and cell temperature. Additionally, it is not advisable to use temperature and irradiance as sensed parameters because doing so would necessitate installing expensive Its measurement seems to be quite expensive, especially for big PV array plants, because equipment is required across the PV array to collect the values of those variables for each panel. [75].

Under every weather circumstance, the direct approaches are effective. The most popular direct MPPT techniques are P&O, InC, and FL-based. Commercially available devices frequently employ perturbative MPPT techniques like P&O and InC to determine, instant by instant, the voltage and current value at which the PV array module produces its maximum power [49–61]. These two techniques have the following key benefits: they can be used with any PV array generator, they don't require knowledge of the PV array generator, and they are easy to implement on a digital controller. These techniques can also be used into industrial inverters. Under static and dynamic situations, P&O and InC both exhibit almost equal tracking capabilities. Both of them are based on the same mathematical relationship between the power derivative and voltage. As a result, InC is viewed as a particular implementation of the P&O algorithm rather than as a distinct MPPT. [76]. Many MPPT algorithms are developed to track the global MPP instead of the local MPP, in the case of partial shading and degradation phenomena of a PV array module [68, 77-84]. Various standards are followed to meet the MPPT efficiency requirements of the converters; e.g. IEC/IS 61683 for standalone PV array systems, and EN 50530/IEC 62891 for grid-interactive PV array systems [85-89], as indicated in Table 2.3.

2.7 Conclusion

This chapter has presented the history and development of EV single stage charging system. An extensive literature review has revealed the shortcomings of existing technologies in terms of complexity, expensiveness, unreliable and inefficiency. Many research areas have been identified to overcome this drawback of currently deployed technologies. Furthermore, the standards and quality certifications (international and Indian) required for the solar PV array have been depicted in detail.

CHAPTER 3

MODIFIED ZETA BASED ISOLATED INTEGRATED CONVERTER

3.1 Introduction

This chapter focuses on a new power electronic converter for PEVs that is capable of operation for all three modes. schematic of the developed isolated integrated converter is shown in Fig.3.1. The suggested arrangement is taken from a conventional Zeta converter, which acts as a conventional boost and buck converter in propulsion and regenerative braking modes, respectively, and as a conventional Zeta PFC during plug-in charging mode. The battery may be charged from any input voltage because Zeta operates in plug-in charging mode. Additionally, due to the ability to buck/boost in this mode as well, the energy stored in the spinning components may be fully collected during regenerative braking. Additionally, this converter has fewer parts than other converters now on the market that can buck and boost in all modes. The controller implementation in this converter is made easier by the fact that just one switch is active throughout each model. A thorough stress and loss study of the converter has also been looked into, for choosing semiconductor components and demonstrating the viability of the suggested converter.

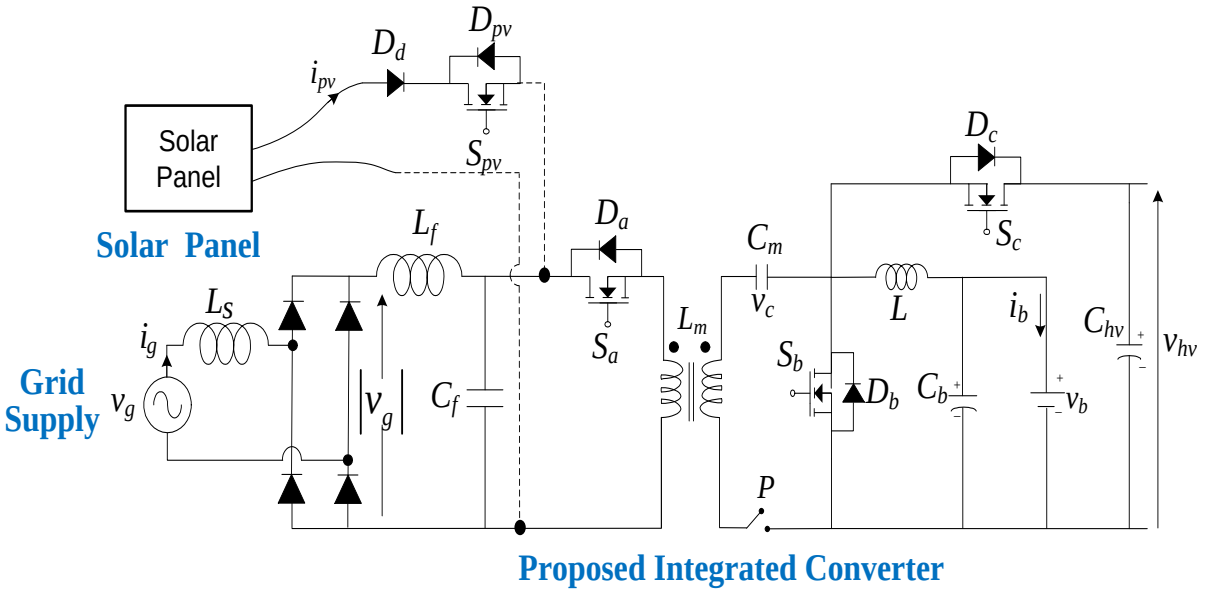

Figure 3.1. Integrated converter for PEV battery charger developed.

3.2 Conventional ZETA Converter

Fig. 3.2 demonstrations circuit arrangement of conventional ZETA converter for PFC operation. The converter can operate in either Current conduction mode (CCM) or discontinuous conduction mode (DCM). But for high power applications, e.g., PEVs, the DCM operation is not preferred because of high current stress produced in semiconductor devices which in-turn will necessitate use of high current rating devices. In addition, when converter operates in DCM, the electromagnetic interference (EMI) problem increases which may cause malfunctioning of other systems too. Therefore, the CCM operation of the converter is more prevalent for high power applications. Only was plug-in charging mode is feasible with a typical ZETA converter's single switch; the other modes (propulsion and regenerative braking) need the use of one or more extra components.

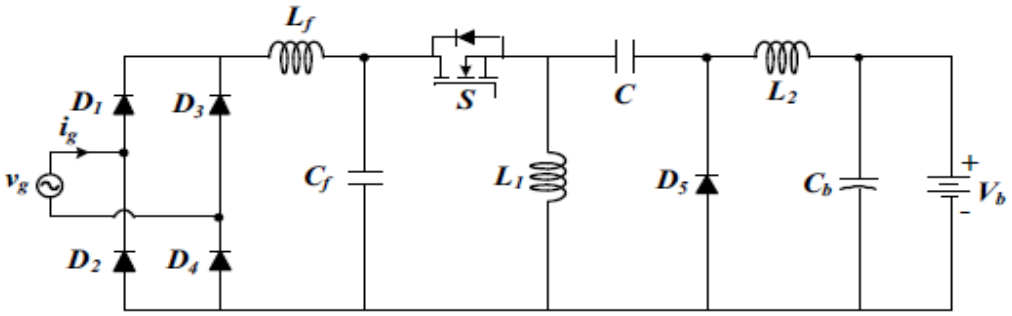

Figure 3.2. Conventional ZETA converter for power factor correction

3.2.1 Characteristics of Proposed Integrated Converter

A novel grid- and solar-based single-stage isolated integrated converter is presented in this study for on-board applications based on the literature research, as illustrated in Fig. 3.1. The main characteristics of the suggested charging system are as follows: (a) the ability to operate the charger with two different power sources (grid and solar PV), which increases charger reliability; (b) the ability to operate all PEV operational modes with a single converter; (c) galvanic isolation between the battery and the power sources for improved user safety and charging, circuit protection (d) lower electricity costs for per-unit charging. The suggested remedy was created using a standard zeta converter, which functions as an isolated zeta for solar PV charging and plug-in charging modes, respectively. Additionally, the suggested integrated converter functions as a boost converter and a buck converter, respectively, in propulsion and regenerative braking modes. The next Section gives an explanation of how the suggested integrated converter works.

3.3 Principle of the Proposed Integrated Converter

Three switches, four diodes, three capacitors (excluding the filter capacitor), two inductors (excluding the filter inductor), and one high-frequency transformer make up the proposed integrated converter in Fig. 3.1. Table 3.1 lists the states of semiconductor devices in each mode. The converter's functioning is covered using operational waveforms in the following sections.

3.3.1 Plug-in Charging Mode

Only when the solar panel's output falls below a certain threshold does this mode activate. The suggested integrated converter is operating as an isolated zeta converter in this scenario since the switch "S_{PV}" is deactivated and only the grid supply is used to charge the batteries. When the manual switch *"P"* is closed, the pulse width modulation (PWM) signal is applied to the semiconductor switch *"S_a"* making it active. Following the path given by the dotted lines in Fig. 3.3, the magnetizing inductor *"L_m"* stores and releases energy to charge the battery through a capacitor *"C_m"* and an inductor *"L"* Additionally, just diode *"D_b"* is used in this mode, and switches *"S_b"* and *"S_C"* are open-circuited.

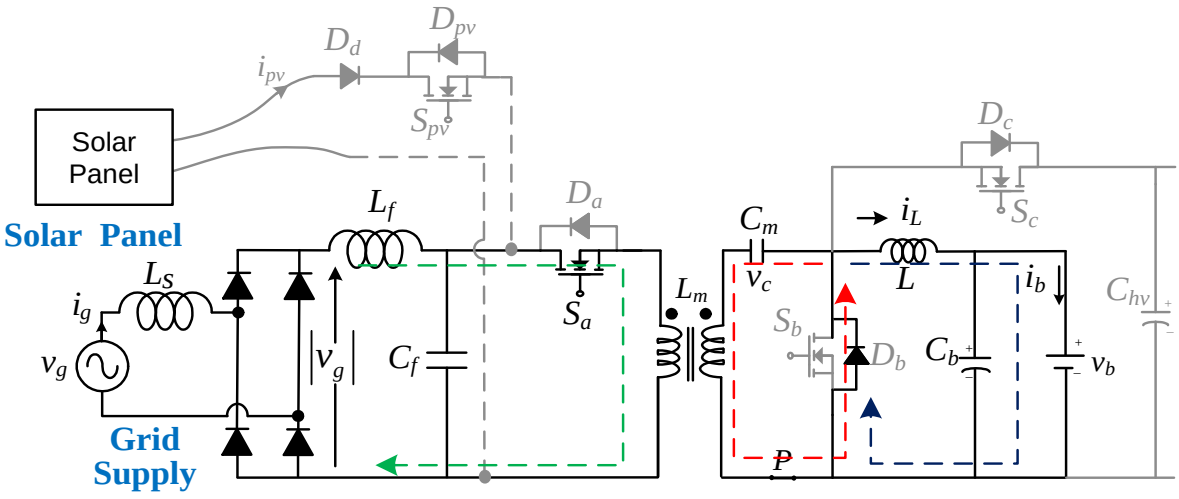

Figure 3.3. utilising a plug-in grid source to charge the battery.

Considering that d_1 is the duty cycle in this charging mode, the voltage-sec. equalizing concept for inductors L_m /L over one switching duration T_s can be written as,

$$V_{g\max}\,|\sin(\omega t)|\times d_1(t) = V_b\times\{1-d_1(t)\}\times T_s \tag{3.1}$$

Using eq. (3.1), the voltage transfer function M_1 can be expressed as,

$$M_1=\frac{V_b}{V_{g\max}\,|\sin\omega t|}=\frac{d_1(t)}{1-d_1(t)} \tag{3.2}$$

3.3.2 Solar PV Charging Mode

When a solar panel's output power exceeds a certain threshold, this mode becomes active. Switch *"P"* and the semiconductor switch *"S_a"* are both closed in this instance, but switches *"S_b"* and *"S_C"* are not in use. In this mode, the converter improves the performance of the PV panel in all weather circumstances by generating the switching signal for the switch *"S_a"* using MPPT management. Fig. 3.4 shows the analogous circuit for this operating mode. The voltage conversion ratio is the same as the previous one since the same converter setup is employed in this mode as well.

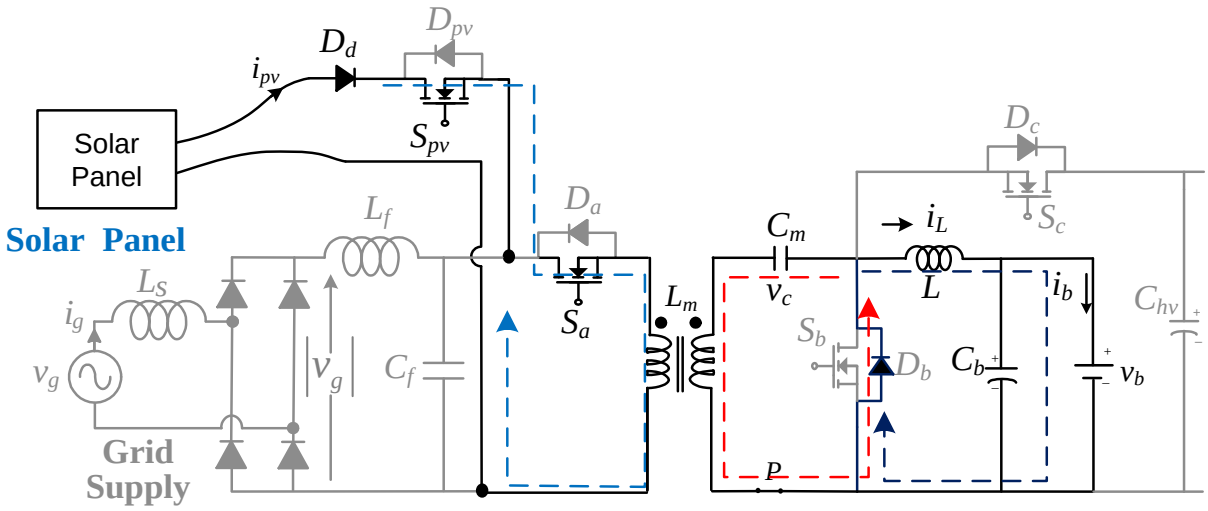

Figure 3.4. Charging of the battery using solar power.

3.3.3 Propulsion Mode

When this mode begins, the battery activates a voltage source converter to deliver power to the propulsion engine. In this mode, the SPST switch *"P"* is open-circuited, and while switch *"S_b"* is operating through a PWM signal, semiconductor switches *"S_a"* and *"S_c"* remain permanently in the open position. As shown in Fig.3.5, while the switch *"S_b"* is closed, the inductor *"L"* charges through the path *"V_b-L_1-S_b-V_b"* (red dotted line), and when *"S_b"* is inactive, the inductor *"L"* transfers its energy to the propulsion motor via the diode *"D_c"* (blue dotted line).

All the elements taking part in this mode make the boost structure. Considering that d_2 is the duty cycle in this mode, the average inductor voltage over one switching duration, T_s, is zero and hence,

$$\left(V_b - V_{hv}\right)\left(1 - d_2\right)\times T_s = V_b \times d_2 \times T_s \tag{3.3}$$

Using eq. (3.3), the voltage transfer function M_2 can be expressed as,

$$M_2 = \frac{V_{hv}}{V_b} = \frac{1}{1 - d_2(t)} \tag{3.4}$$

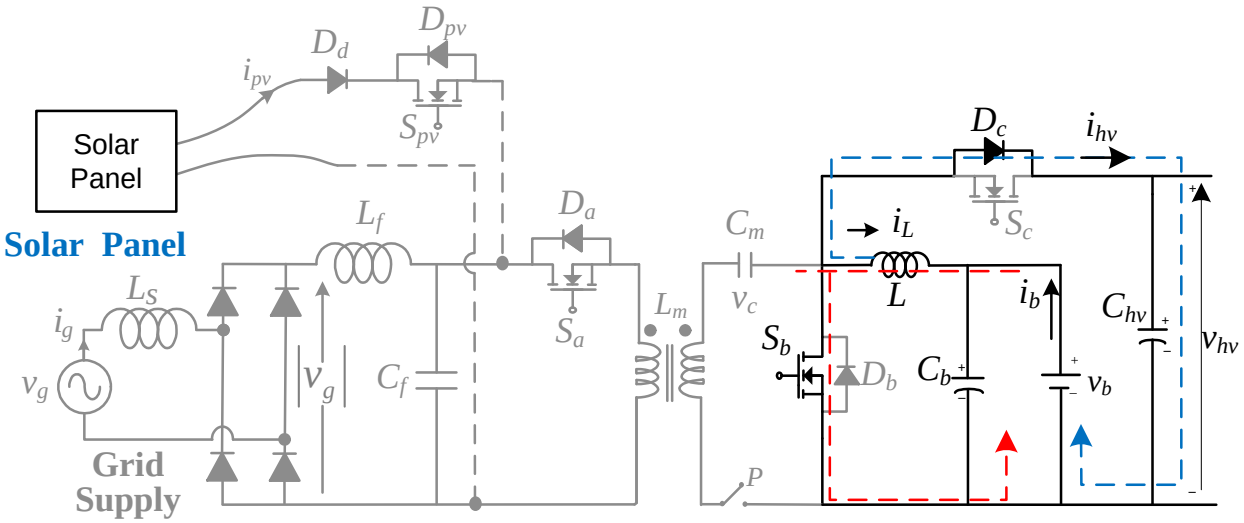

Figure 3.5. Operation in the propulsion mode.

3.3.4 Regenerative Braking Mode

In this mode, the propulsion motor drive's regenerative recovery power is used to charge the battery. The PEV's driving range is ultimately increased by this phenomenon The switch *"P"* remains open while in this mode, the switch *"S_C"* is turned on. The *"S_a" and "S_C"* switches, both are inactive in this mode. Fig. 3.6 depicts the proposed converter's operation in this mode.

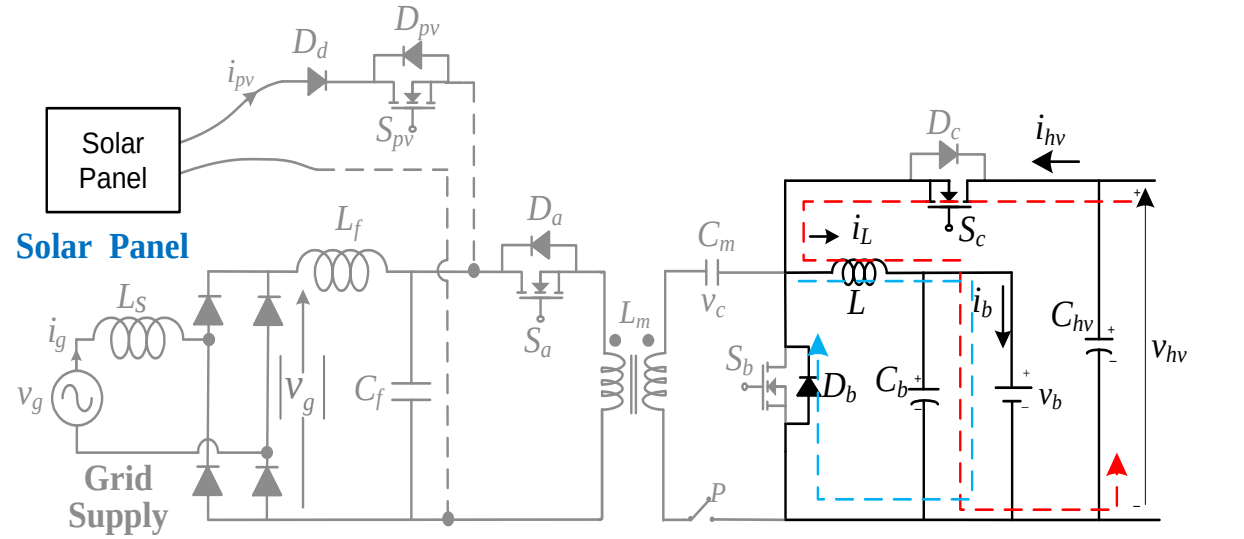

Figure 3.6. Operation in the regenerative recovery mode.

Based on the average inductor voltage during one switching duration, eq. (3.5) is derived, and the voltage transfer function M_3 can be expressed as (3.6).

$$\left(V_{hv} - V_b\right) d_3 \times T_s \;=\; V_b \times \left(1 - d_3\right) \times T_s \tag{3.5}$$

$$M_3 = \frac{V_b}{V_{hv}} = d_3(t) \tag{3.6}$$

Table 3.1

States Of Semiconductor Devices in Various Modes.

Operating Mode	S_a	S_b	S_c	S_{pv}	D_a	D_b	D_c	D_{pv}
PGC	1	0	0	0	0	1	0	0
PV	1	0	0	1	0	1	0	0
PR	0	1	0	0	0	0	1	0
RB	0	0	1	0	0	1	0	0

*1: Closed and 0: Open.

3.4 Voltage/Current Estimation for Component Selection

The proposed integrated converter operates in bidirectional mode, and hence few of the power devices are common in AC-to-DC or DC-to-DC conversions. Therefore, the stresses on the semiconductor components in terms of voltage and current can be diverse in different working modes due to dissimilar ratings. The particular semiconductor switch/diode is chosen by maximum voltage/current magnitudes appearing during various operations. Table II indicates the maximum voltage/current stresses onto the switches/diodes in each working mode. Using this table, the ratings of switches are chosen as follows:

The maximum voltage rating of the switch is

$$S_a = [v_g(\omega t)_{\omega t=\pi/2} + V_b] \tag{3.7}$$

and the maximum rating in terms of current for the S_a switch is,

$$S_a = i_g(\omega t)_{\omega t=\pi/2} + I_b \tag{3.8}$$

whereas the maximum voltage ratings of switches $S_b$and S_c are S_b & S_c = max (V_{hv} V_b). On the other hand, the current magnitudes of S_b and S_c are selected by the propulsion mode power requirement, since this working mode requires the maximum power compared with the rest of the modes.

Table 3.2

Maximum Voltage/Current Ratings Of Switches And Diodes

	$S_a\,(D_a)$		$S_b\,(D_b)$		$S_c\,(D_c)$	
Operations	Voltage	Current	Voltage	Current	Voltage	Current
Charging (PGC & PV)	$\left[v_g(\omega t)_{\omega t=\pi/2}+V_b\right]_{S_a}$	$\left[i_g(\omega t)_{\omega t=\pi/2}+I_b\right]_{S_a}$	$\left[v_g(\omega t)_{\omega t=\pi/2}+V_b\right]_{D_b}$	$\left[i_g(\omega t)_{\omega t=\pi/2}+I_b\right]_{D_b}$	$\left[v_g(\omega t)_{\omega t=\pi/2}+V_b\right]_{D_c}$	NO
PR	$[\text{Zero}]_{S_a(D_a)}$	NO	$[V_b]_{S_b}$	$\left[\langle i_{Lprop}\rangle_{T_s}+\frac{\Delta i_{Lprop}}{2}\right]_{S_b}$	$[V_{hv}]_{D_c}$	$\left[\langle i_{Lprop}\rangle_{T_s}+\frac{\Delta i_{Lprop}}{2}\right]_{D_c}$
RB	$[\text{Zero}]_{S_a(D_a)}$	NO	$[V_b]_{D_b}$	$\left[\langle i_{Lrege}\rangle_{T_s}+\frac{\Delta i_{Lrege}}{2}\right]_{D_b}$	$[V_{hv}]_{S_c}$	$\left[\langle i_{Lrege}\rangle_{T_s}+\frac{\Delta i_{Lrege}}{2}\right]_{S_c}$

Additionally, to examine the losses in different modes, the current stress model is required. Thus, the stress in terms of current through the semiconductor devices is established in charging methods, and equivalent examination can be anticipated for the rest of the working modes:

3.4.1 Switch "S_a" Current And Its Rms Value:

$$i_{s_a,RMS}=\sqrt{\frac{1}{T_L}\int_0^{T_L}\langle i^2{}_{s_a}\rangle_{T_s}\,dt} \tag{3.9}$$

$$\langle i^2{}_{s_a}\rangle=\frac{1}{T_s}\int_0^{t+T_s} i^2{}_{s_a}(t)\,dt=d_1(t)[i_{Lm}(t)+i_L(t)]^2 \tag{3.10}$$

where $d_1(t) = 1/\ 1+\alpha\ sin(\omega t)$, using (2) and $\alpha = V_{gmax}\ /V_b$. The currents flowing through the inductors $(L_m$ *and* $L)$ can be expressed as: $i_{Lm}(t) = I_{g,max}\cdot sin(\omega t)$ *and* $i_L(t) = \alpha I_{g,max}\cdot sin^2(\omega t)$. Based on the $d_1(t)$, $i_{Lm}(t)$ and $i_L(t)$, eq. (9), can be reformulated as,

$$i_{s_a,RMS}=I\sqrt{\frac{1}{\pi}\int_0^{\pi} sin^2(\omega t)[1+\alpha\,sin(\omega t)]\ d(\omega t)}$$

$$=I\sqrt{1+\alpha\frac{8}{3\pi}} \tag{3.11}$$

An analogous investigation for an RMS current of the diode D_a produces the following equation:

$$i_{D_a,RMS}=I_b\sqrt{\frac{3}{2}+\alpha\frac{16}{3\pi}} \tag{3.12}$$

3.4.2 Manual Switch "P" Current And Its Rms Value: The magnitude of current flowing through the manual switch "*P*" is similar to that of the current-carrying by the middle capacitor C_m. Therefore, the RMS current through *P* is exactly the same as the current through the switch S_a and can be expressed as,

$$i_{p,RMS} = \sqrt{\frac{1}{\pi}\int_0^{\pi}[d_1(t)\{i^2{}_L\} + (1 - d_1(t))\{i^2{}_{Lm}\}]\, d(\omega t)} \tag{3.13}$$

$$i_{p,RMS} = I\sqrt{\frac{1}{\pi}\int_0^{\pi}[\alpha\, sin^3(\omega t)]\; d(\omega t)} = I_{g,RMS}\sqrt{\alpha\frac{8}{3\pi}} \tag{3.14}$$

3.4.3 Average Currents of the Diode D_b and Switch S_a:

The average diode current flowing through diode D_b is expressed as,

$$i_{D_b,avg} = \frac{1}{\pi}\int_0^{\pi}(1 - d_1(t))[i_{Lm}(t) + i_L(t)]d(\omega t) \tag{3.15}$$

$$i_{D_b,avg} = \frac{I_{g,max}}{\pi\int_0^{\pi}[\alpha\, sin(\omega t)]d(\omega t)} \tag{3.16}$$

$$i_{D_b,avg} = \frac{I_{g,RMS}2\sqrt{2}}{\pi}\;\alpha \tag{3.17}$$

In addition, the average currents flowing through the switch S_a can be obtained as:

$$i_{s_a,avg} = I_{g,RMS}\frac{2\sqrt{2}}{\pi} \tag{3.18}$$

3.5 Design of the Proposed Converter

Generally, the power ratings of converter devices in each operating mode of the vehicle vary and cannot be the same. So, the choice of switch ratings for the converter entirely depends upon the specific operating mode. The rating (voltage and current) of these devices is determined based on stresses in the switching devices.

3.5.1 Selection of Switching Devices

Due to bidirectional operation in the dc/dc stages some of the diodes and switches are pooled between the ac/dc and dc/dc stages. In arrears to the varied power and voltage capabilities of various modes, the voltage and current rinsing on switches and diodes may vary depending on the mode.Therefore, the peak voltage/current option for a certain switch determines the voltage/current rating option. generated in the switch or its body diode during any mode. Table 3.2

shows the peak voltage and current strains on switches in each mode. These choices are made for switch rating from this Table3.2:

The peak voltage rating of Sa is given as: $S_a = [v_g(\omega t)_{\omega t=\pi/2} + V_b]$, and Sa has a maximum current rating of $i_g(t)t=/2 + I_b$. while switches $S_b$and S_c have maximum voltage ratings of S_b& S_c = max (V_{hv}, V_b). While the propulsion mode power rating determines the current S_a and S_b ratings.

3.5.2 Selection of Passive Components

Inductor L_2 participates in all mode of converter operation. Therefore, the CCM condition of the converter for each mode can be ensured by selecting the inductor value for each of these modes with allowable current ripple. The maximum of these computed values is picked up as the value of inductorL_2.

The value of L_2 for CCM operation in plug-in charging mode is given as [91],

$$L_2 > \left(\frac{R_L d'_1(t) T_s}{2} \right) > \frac{R_{L,\max}}{2} \frac{\left|V_{g,\max}\right|}{\left|V_{g,\max}\right| + V_b} \frac{1}{f_s} \tag{3.19}$$

Using parameters given in Table 3.3 value of *'L_2'* in plug-in charging mode is calculated as,

$$L_{2\,plug-in} > \frac{90}{2} \frac{311}{311+300} \frac{1}{20000} = 1.14mH \tag{3.20}$$

The values of L_2 for CCM The following equation describes functioning in propulsion and regenerative braking modes: [3.18 3.19],

$$L_{2\,prop} = \frac{V_b d_2}{\Delta i_b f_s} \tag{3.21}$$

$$L_{2reg} = \frac{V_b (1-d_3)}{\Delta i_b f_s} \tag{3.22}$$

where Δi_b is the battery ripple current. Using parameters given in Table 3.3 and choosing battery ripple current Δi_b = 20 % of I_b, value of L_{2prop} and L_{2reg} is calculated as

$$L_{2reg} = L_{2reg} = \frac{300 \times 0.25}{1.33 \times 20000} = 2.83mH$$

The final value of L_2 is selected as,

$$L_2 = \max\left(L_{2\,plug-in}, L_{2\,pop}, L_{2reg} \right) \tag{3.23}$$

3.5.3 Selection of Capacitor C_m

The coupling capacitor *"C_1"* is an essential part of the recommended converter since its value has a considerable impact on the quality of the input current. As a result, the following limitations will be applied to the design of this capacitor in order to prevent input applications as diverse at each half-line cycle and to maintain constant voltage during such a switching period, the resonance frequencies of *"L_2"* and *"C_m"* during CCM operation must be larger than *"f_l"* the line frequency. and less than the switching frequency, *"F_s"*.

$$f_L < f_r < f_s \tag{3.24}$$

Where,

$$f_r = \frac{1}{2\pi\sqrt{(L_1 + L_2)C}} \tag{3.25}$$

The switching frequency in this work is set at 20 kHz for "F_s" and 1 kHz for "F_r." Both in simulation and in hardware, the capacitor "C_1" is set to 10 F. Because the voltage specification of such a capacitor was chosen on the basis on the battery voltage range, and in all operations the voltage across the coupling capacitor follows the battery voltage.

3.5.4 Selection of Capacitor, C_b

As a capacitor, C_b is connected directly across the battery pack; the higher order of switching harmonics are considered to be negligible. However, the voltage ripple of frequency double to the line frequency is appeared and significantly affects the life of the battery pack. The lower order frequency voltage ripple on V_b is expressed as,

$$\Delta v_b \geq \frac{P_b}{4 f_g C_{b,\min} V_b} \tag{3.26}$$

where, *'F_g'* is the grid supply frequency, and Δv_b is the amount of ripple in the capacitor, 'C_b'. The designed values of the proposed integrated converter utilized in the present system are given in Table 3.3.

Table 3.3

Simulation parameters

Parameters	Values
DC link voltage (V_{hv})	400/60 V
Grid voltage ($V_{g,min}$-$V_{g,max}$)	70.7-220V
Grid Frequency (f_g)	50 Hz
L_2	3 mH
C_b /C_1/ C_{hv}	1500/10/550µF
Switching frequency, (f_{sw})	20kHz
Nominal charging power, (P_b)	1kW/300W
Nominal battery voltage, (V_b)	320/36V
Switches	N-Channel Power MOSFET, IRFP-460

3.6 Control Strategy

Fig. 4.7 exhibits a generalised block diagram of the controller employed by the proposed converter. The integrated converter has three modes of operation, and various control techniques are used in each mode. The mode picker logic first chooses the mode of operation, and then it establishes the baseline quantity for that mode.

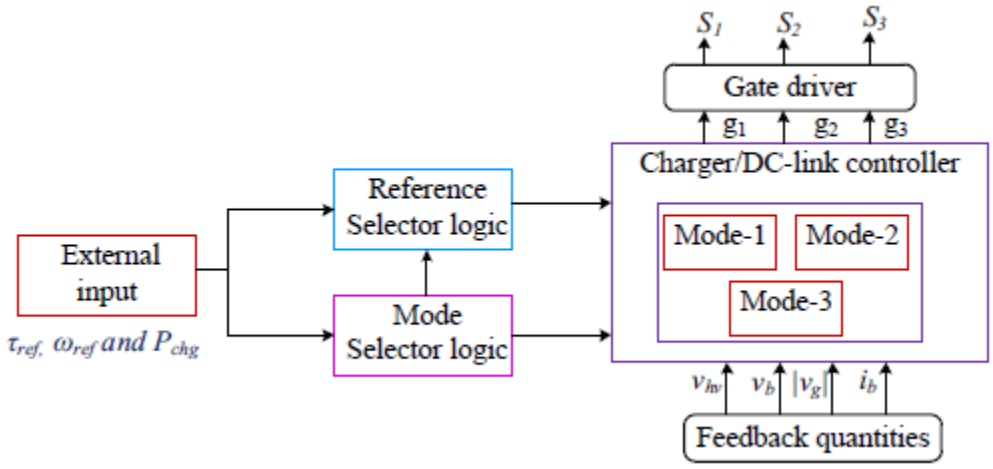

Figure 3.7. General control diagram of the proposed integrated converter

Because depending on the mode of operation, the input reference might be dc bus voltage, charging power, or torque, previous knowledge of the reference amount is required. The concerned controller becomes active and guarantees that the controlled variable follows the reference value after the operating mode and reference amount have been specified. The suggested system's overall control strategy may be divided into two main categories. The PGC and solar PV modes are controlled for charging in the first section, while the second part is to control the PR and RB modes.

3.6.1 Control of Charging Modes (PGC and Solar PV Modes)

This sub-control system includes the PGC and solar PV modes realized by a source selector logic. In the PGC mode, a 2-loop controller is utilized to charge the LPEV and to achieve the power factor correction at the grid side at the same time. The desired battery current is compared with its actual value, and the difference is passed through a controller '$G_{ib}(z)$' as,

$$G_{ib}(Z) = K_p + \frac{K_i\ T_s}{z-1} \tag{3.27}$$

The current reference for G_{iL} is created by multiplying the output of the $G_{ib}(z)$ by a unit template of the sinusoidal signal. The current reference for the G_{iL} controller is built by multiplying the output of the $G_{ib}(z)$ by a unit template of the sinusoidal signal. At the utility grid, it creates the gating signal for "Sa" after power factor compensation. $G_{iL}(z)$ can be written as the expression,

$$G_{iL}(Z) = K_{pc} + \frac{K_{ic}\ T_s}{z-1} \tag{3.28}$$

The gains (K_{pc} and K_{ic}) should be adjusted ensuring that among 1/6th and 1/10th of the operating switching frequency is kept for the controller's bandwidth. Likewise, the $G_{ib}(z)$ controller's bandwidth is configured to less than 120 Hz to limit the disruption in the reference signal for the inner current loop attributable to second harmonic components, i.e., the 120 Hz signal present in battery current. In the solar PV charging mode, the MPPT drift-free P&O (perturb and observe) control approach [11] is utilized to generate the switching pulses for the switch S_a, whereas the switch S_{pv} is turned on/off by simple 0 and 1 logic through a switch selector. Therefore, the losses associated with S_{pv} are minimal.

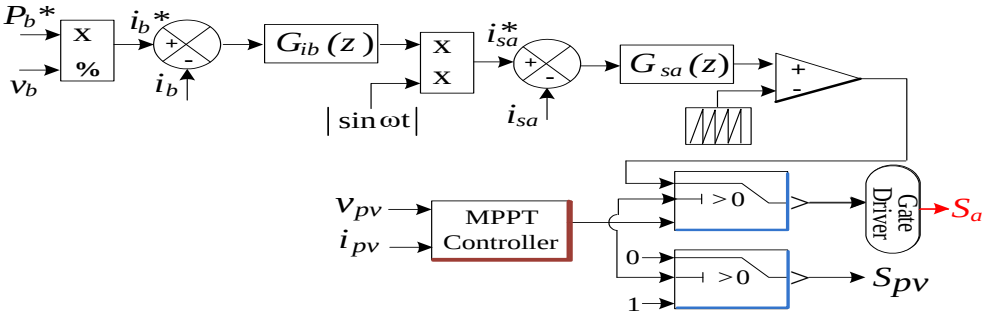

Figure 3.8. Charging of the battery using solar power.

3.6.2 MPPT Control of Solar PV Array With Proposed Integrated Converter

An efficient and commonly used method to perturb and observe MPPT technique consequently, a variety of PV array-dependent applications are used to maximize PV array power under all operational circumstances. An PV array voltage or duty cycle may both be perturbed using this method. The step size and perturbation frequency of the P&O MPPT approach have an impact on its performance.. As follows is the definition of duty cycle perturbation: [62-68],

$$\left.\begin{aligned} &D(k) = D(k-1) + \Delta D \\ &if,\ dp_{pv} > 0 \,\&\, dv_{pv} > 0 \\ &or,\ dp_{pv} < 0 \,\&\, dv_{pv} < 0 \end{aligned}\right\} \tag{3.29}$$

And,

$$\left.\begin{aligned} &D(k) = D(k-1) - \Delta D \\ &if \quad dp_{pv} > 0 \,\&\, dv_{pv} < 0 \\ &or,\ dp_{pv} < 0 \,\&\, dv_{pv} > 0 \end{aligned}\right\} \tag{3.30}$$

someplace, Δv_{pv} is the size of perturbation, and ΔD represents the perturbation size of the duty cycle. Thus, based on the relationship between change in PV array voltage and power, this same controller chooses the perturbation's direction, as seen in Fig. 3.8, and adjusts the duty cycle in accordance.

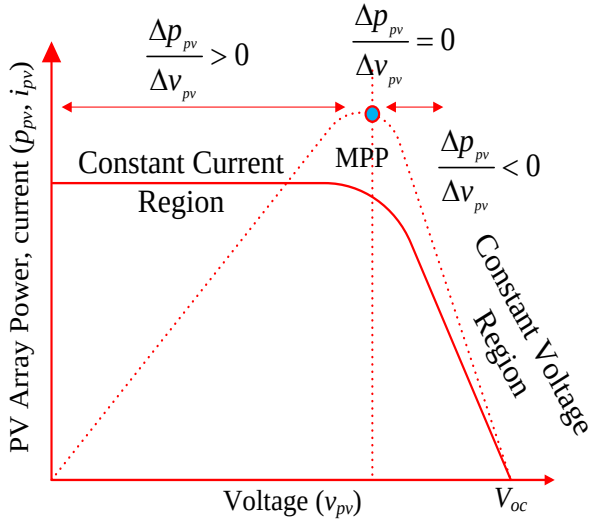

Figure 3.9. PV array characteristics and an example of P&O MPPT.

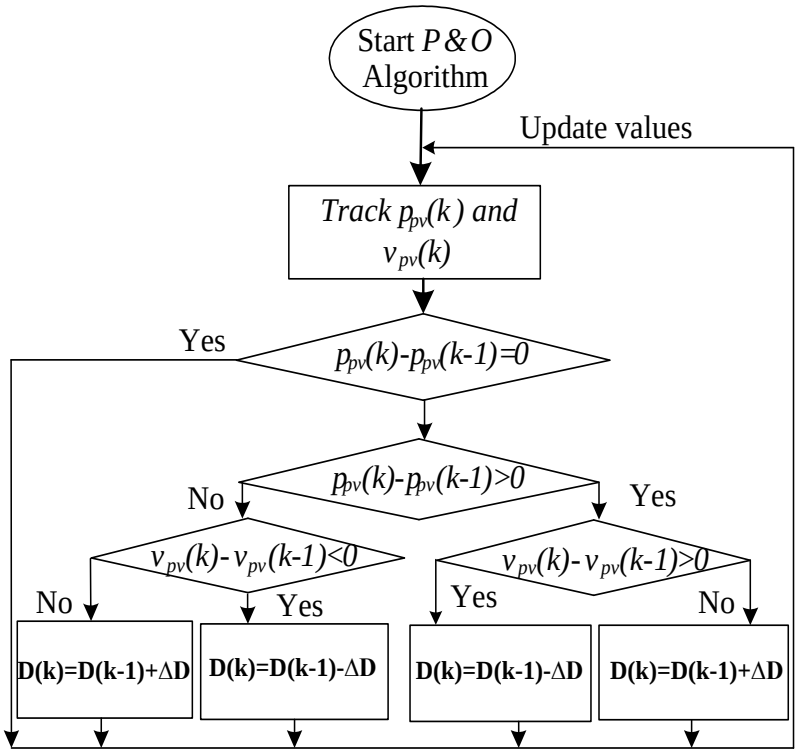

Figure 3.10. Flow-chart diagram of P&O MPPT algorithm.

A controller needs more time to track the MPP of the PV array as the perturbation size decreases. The flow-chart diagram of implemented P&O MPPT algorithm is presented in Fig. 3.10 A high perturbation size results in a faster tracking but at the cost of increased oscillations around the MPP. To achieve the goals of MPPT, an intelligent settlement between the tracking time and the perturbation size is maintained. In order to ease gentle charging of the battery and reduce oscillations around the MPP, the beginning duty cycle is taken as 0.05 and MPPT step size is set at 0.0015.

3.6.3 Control Strategy For Propulsion And Regenerative Braking Modes

For both PR and RB modes, an average current mode control logic is implemented. Based on the working mode, suitable switches are activated using a mode selector. The mode selector logic is a combination of logic gates and identities such as a braking command and the converter input voltage. In the case of propulsion (PR), the input of VSC voltage is regulated utilizing a controller $G_{hv}(z)$ with an inner loop controller $G_{ibc}(z)$.

In the RB mode, apart from the motor inverter switches, the switch S_c plays an active role in recovering the energy from the motor. The switch S_c has PWM pulses generated by the logic shown in Fig. 3.11. The reference input in this mode is the brake torque command. This command then

acts as a reference for the power level of the battery using a PI controller $G_t(z)$ that generates a current reference for the battery pack, as illustrated in Fig. 2.7

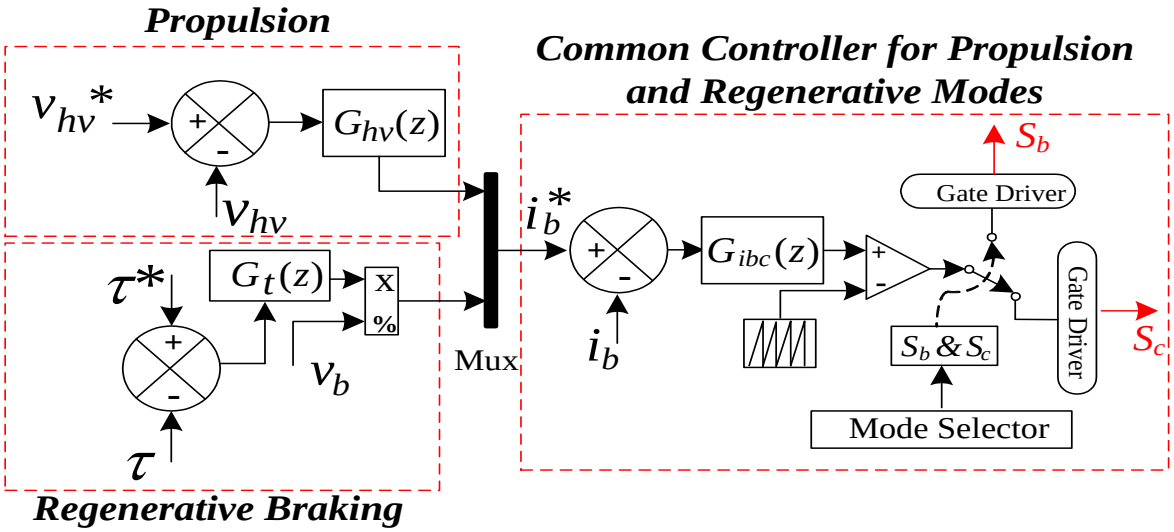

Figure 3.11. Control block diagram of the converter in propulsion and regenerative braking modes.

3.7 Results and Discussion

The proposed converter is simulated in a MATLAB/Simulink scenario using the converter's parameters, which are listed in Table 3.1. The simulation research for plug-in charging is conducted separately for propulsion and regenerative braking modes. When the battery is charging, The baseline battery voltage is 300 V with 20% SOC, the grid voltage is set to 220 V, and the charging power is 1 kW. Fig. 2.7 displays simulated waveforms for the grid voltage *(V_g)*, grid current *(I_g)*, battery voltage *(V_b)*, battery current *(I_b)*, and grid side filter voltage and current *(V_{cf}* and *I_{cf})*. Grid current and voltage are in phase. They can be shown in Fig. 3.12. Fast Fourier analysis was used to calculate the grid current's total harmonic distortion *(THD)* and power factor *(PF)* is 3.78% and 0.99.

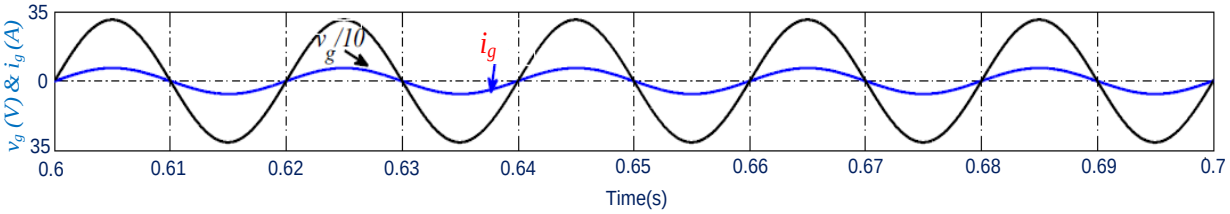

Figure 3.12. Simulation waveforms during plug-in charging mode with 220 V_{RMS} of grid voltage.

In Fig. 3.13, the battery voltage and current are also depicted. As can be observed from Fig. 3.13, a single-stage (single-phase) system's intrinsic low frequency (100 Hz) oscillation of the battery current is present. The filter inductor linked in series with the battery is what causes the battery current to oscillate. A compromise between the allowed the determination of the 1inductance filter's value was based on low frequency battery ripple current and the compactness of the charger.

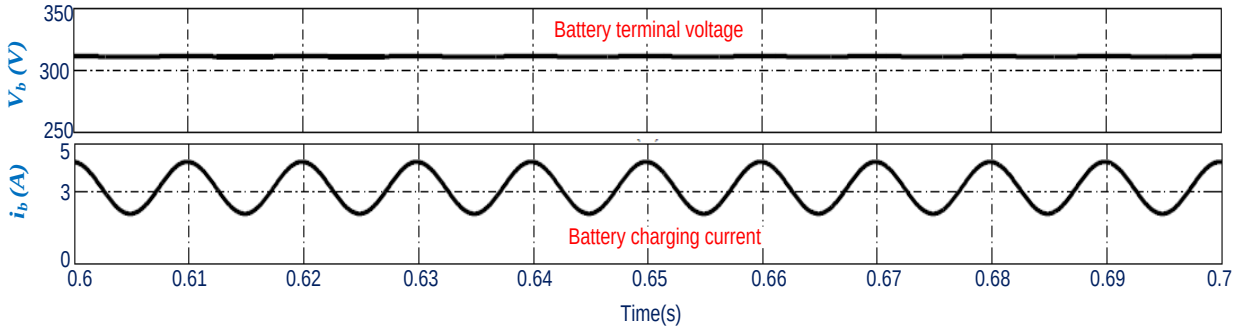

Figure 3.13. Waveforms of battery voltage (V_b) and battery current (i_b) during plug-in charging mode through grid.

The grid side filter capacitor voltage and filter inductor current also showed up here. Fig. 3.14 The voltage across the filter capacitor is seen to be consistent and pulsing.. The filter current is also having same nature with different magnitude. Peak current through L_f is 6.7 A, while the highest voltage across $C_f$is 311 V, complementing the peak grid voltage.

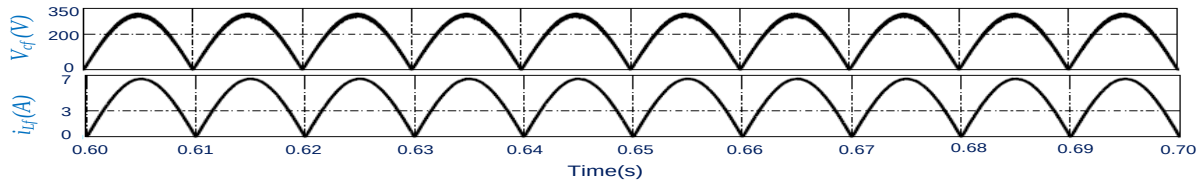

Figure 3.14. Waveforms grid side filter capacitor voltage and filter inductor current during plug-in charging mode through grid.

The THD bar chart of input current is shown in Fig.3.15, where the THD is 3.6%. The UPF operation of the converter lowers the price of energy consumption and also lessens the loss of reactive power in the grid system.

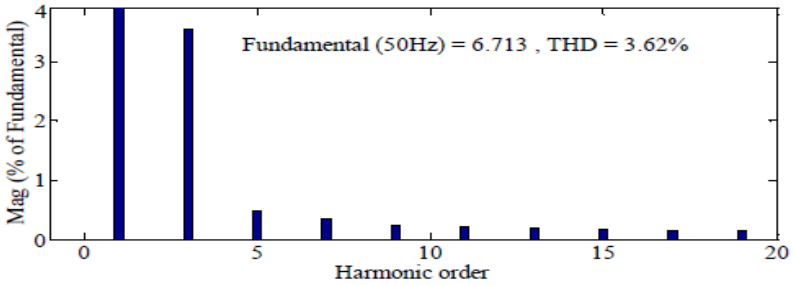

Figure 3.15. THD of grid current

The voltage waveform across capacitor C_m is shown in Fig. 3.16(a). The peak voltage across this capacitor is same as the peak grid voltage (212 V). The voltage across switch S_a is the sum of grid voltage and the battery voltage $(v_g + v_b)$ which is shown in Fig. 3.16(b).

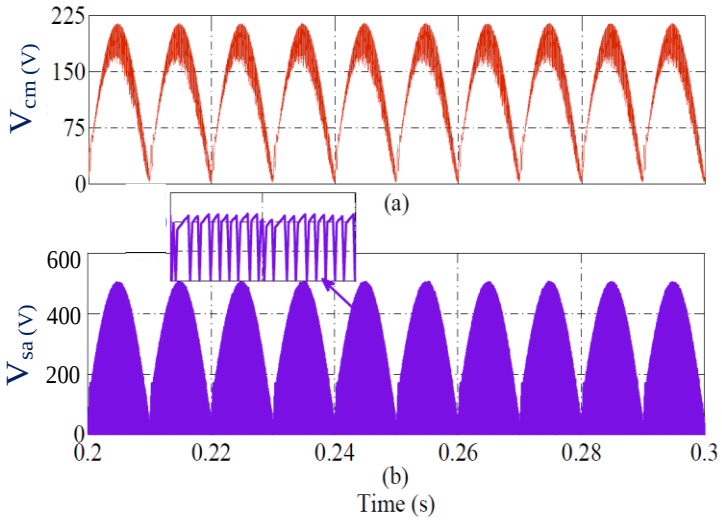

Figure 3.16. Simulation results of the plug-in charging mode (a) voltage waveform across capacitor C_m, (b) voltage waveform across switch S_a.

Since, the proposed system has dual charging mode characteristics. Therefore, the observation of the performance of the solar PV array parameters during the solar charging mode has also been studied and analyzed. The behaviour of solar PV voltage, current and battery terminal voltage under these conditions are displayed in Fig.3.17. The ripple in MPPT voltage is also minimal which helps to optimize the performance of the solar PV panel. Similarly, the solar PV cuurent has also very small ripple and track it sdesired magnitude at this insolation. On the other side, the rated value of battery terminal volatage demostarte the smooth charging of of battery.

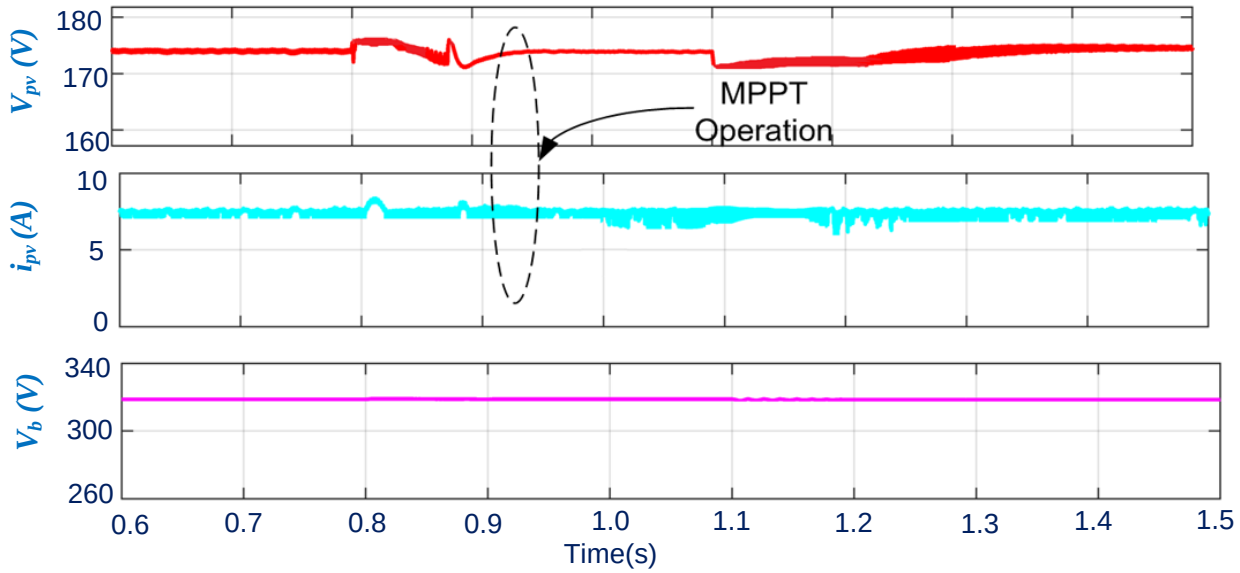

Figure 3.17. Waveforms of PV and battery parameters in solar PV plug-in charging mode.

With a 400 V dc-link and 1 kW of output load power, the proper waveforms of the proposed system in propulsion mode are shown in Figs.3.18 This section's step load adjustments demonstrate the dynamic behaviour of this mode. At t = 1.2 s, At t = 1.8 s, the load power falls to 1 kW from a peak of 2 kW. The dc-link voltage must be kept consistent, which is the control objective of this mode, for the inverter-drive system to operate well. Figure 3.18, which illustrates the efficacy of the controller performance, indicates that the dc-link voltage is well regulated at 400 V after the load changes.

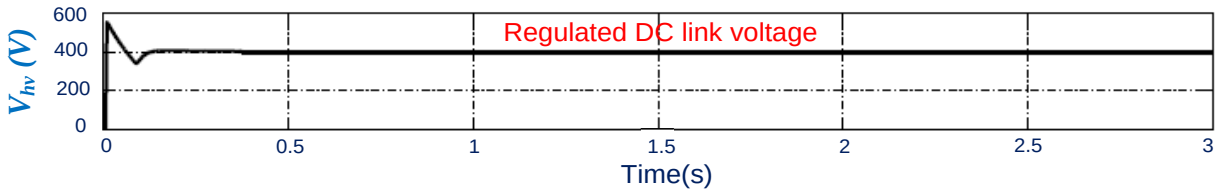

Figure 3.18. Behaviour of DC link voltage in propulsion mode under load change.

The battery voltage and current are shown in Fig. 3.19 The battery current is seen to be increasing from 3.45 A to 6.9 A at t = 1.2 s. Similarly, when load is reduced from 2 to 1 kW at t = 1.8 s, the battery current comes down to 3.45 A from 6.9 A. As seen in Fig. 3.19.the battery voltage is nearly constant during this interval.

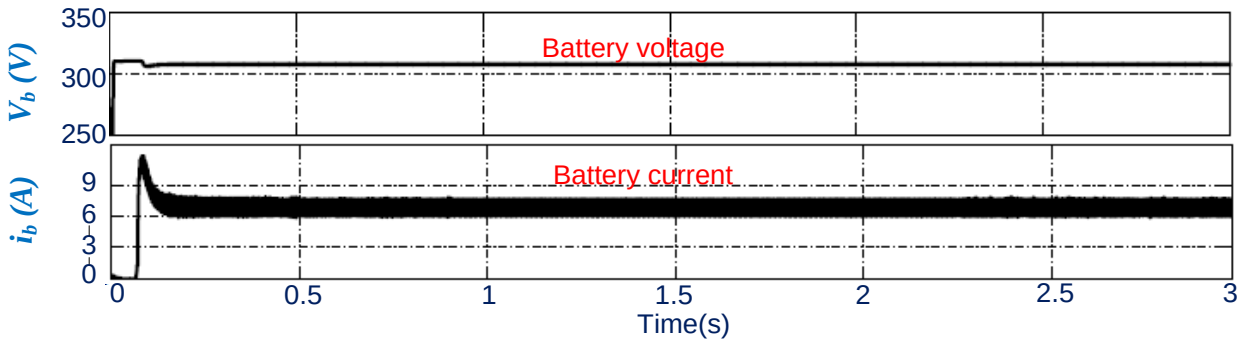

Figure 3.19. Behaviour of battery voltage and current in propulsion mode under load change.

Figs. 3.20 and 3.21 depict the waveforms of the regenerative mode. The battery is charged using just a constant current while the dc-link voltage is changed to confirm this mode. Thus according Fig. 3.21, the dc-link voltage fluctuations range from 290 V to 350 V.

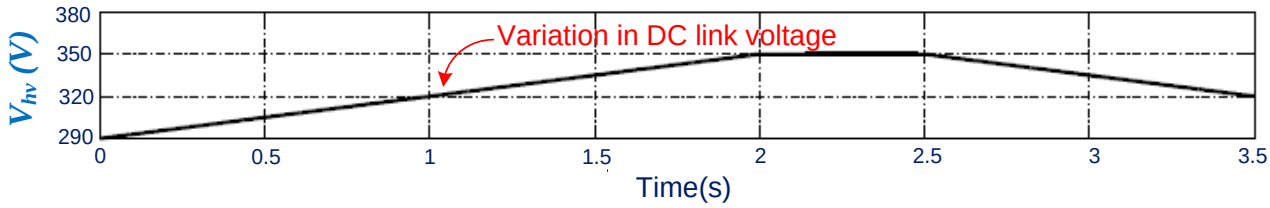

Figure.3.20 . Nature of DC link voltage in regenerative braking mode.

Importantly, Fig. 3.21 displays the battery voltage and current. Regardless of changes in the dc-link voltage, the controller maintains the battery current at 3.5 A..

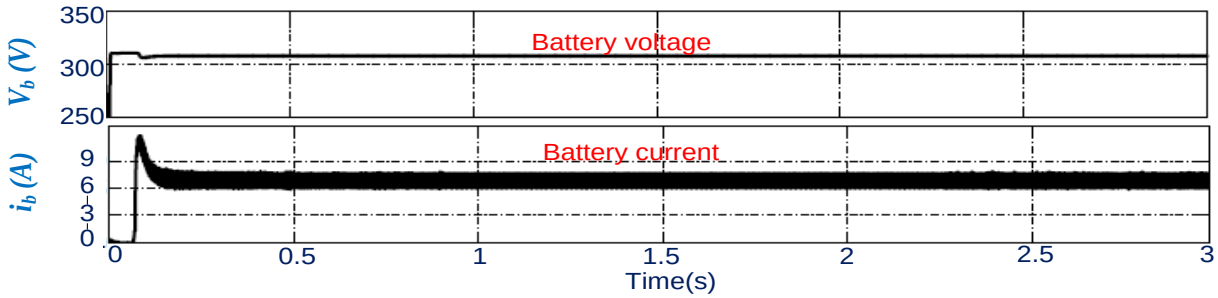

Figure 3.21. Nature of battery voltage and current variation in regenerative braking mode.

3.8 Conclusion

The integrated converter indicated in this article functions as a ZETA converter for plug-in charging and regenerative braking modes, although as a buck mode converter for propulsion mode. As a result, it demonstrates buck/boost capabilities for each of these modes of operation without voltage inversion, allowing for a diverse variety of battery voltage selection, efficient a broad range of motor speeds, dc-link voltage stabilization, and the collection of regenerative braking energy. The suggested converter has fewer components as compared to the single-stage converters that are

already available and have comparable buck/boost capabilities in each mode. Numerous simulation results have been used to confirm the suggested integrated converter's operation and performance. The efficacy of the control method is evaluated using propulsion mode step load swings and regenerative braking mode dc-link voltage variations.

CHAPTER 4

CONCLUSION AND FUTURE SCOPE

4.1 Conclusion

The traditional single-stage chargers only function in charging mode; as a result, additional converters must be used to accomplish other modes, increasing system weight and expense. As a result, OBC applicants do not find these fees appealing. An effective EV charging system with a multi-functional isolated DC-DC converter has been designed for onboard applications in recognition of the shortcomings of traditional chargers. The created technology charges the battery when the vehicle is stationary by using grid and solar electricity in a complimentary manner. Under all operational conditions, the converter's performance is effective. The proposed converter's regenerative brake control method has been explored, and simulation results have confirmed the idea. The integrated converter's planned layout does away with the need for additional switches and inductors for electric powertrain. Relevance analysis and simulation results using MATLAB under various operating situations are used to justify the suggested topology.

4.2 Future Scope

The proposed work presented in this report focuses on converter part of PEVs. Future expansion of presented work in this thesis will include:

- The drive system of the vehicle can be included to interface various types of motors such as induction, BLDC and SRM with the integrated converters.
- Validate the developed charging system in real time environment through experimental set-up.
- Another potential future use of this work is the use of super capacitors with integrated converters that are PV interfaced. The high power density super capacitor may be employed in automobiles in one of two ways: either in conjunction with a battery or alone. Depending on the application, a super capacitor can either be connected directly to the dc-link or through a dc/dc converter when used with a battery.

REFERENCES

[1] C. C. Chan and K. T. Chau, *"An overview of power electronics in electric vehicles," IEEE Transactions on Industrial Electronics, vol. 44,* no. 1, pp. 3–13, Feb. 1997.

[2] A. Emadi, Y. J. Lee, and K. Rajashekara, *"Power electronics and motor drives in electric, hybrid electric, and plug-in hybrid electric vehicles,"IEEE Transactions on Industrial Electronics, vol. 55,* no. 6, pp. 2237–2245, Jun. 2008.

[3] A. K. Singh and M. K. Pathak*, "An improved two-stage non-isolated converter for onboard plug-in hybrid EV battery charger," in 2016 IEEE 1st International Conference on Power Electronics, Intelligent Control and Energy Systems (ICPEICES),* pp. 1–6, Jul. 2016.

[4] F. Musavi, M. Edington, W. Eberle, and W. G. Dunford, "Evaluation and efficiency comparison of front end AC-DC plug-in hybrid charger topologies*," IEEE Transactions on Smart Grid,* vol. 3, no. 1, pp. 413–421, Mar. 2012.

[5] B. P. McGrath, D. G. Holmes, P. J. McGoldrick, and A. D. McIver, "Design of a soft switched 6-kw battery charger for traction applications," *IEEE Transactions on Power Electronics,* vol. 22, no. 4, pp. 1136–1144, Jul. 2007.

[6] C. C. Chan and K. T. Chau, *"Power electronics challenges in electric vehicles,"* in Industrial Electronics, Control, and Instrumentation, 1993. Proceedings of the IECON '93. *International Conference* on, pp. 701–706 vol.2, Nov. 1993.

[7] I. A. Khan, "Battery chargers for electric and hybrid vehicles," in Proceedings of *1994 IEEE Workshop on Power Electronics in Transportation,* pp. 103–112, Oct. 1994.

[8] J. C. Gomez and M. M. Morcos, "Impact of EV battery chargers on the power quality of distribution systems*," IEEE Transactions on Power Delivery,* vol. 18, no. 3, pp. 975–981, Jul. 2003.

[9] F. L. Mapelli, D. Tarsitano, and M. Mauri, "Plug-in hybrid electric vehicle: Modeling, prototype realization, and inverter losses reduction analysis," *IEEE Transactions on Industrial Electronics,* vol. 57, no. 2, pp. 598–607, Feb. 2010.

[10] M. M. Morcos, N. G. Dillman, and C. R. Mersman, "Battery chargers for electric vehicles," *IEEE Power Engineering Review, vol. 20,* no. 11, pp. 8–11, 18, Nov. 2000.

[11] J. Dixon, I. Nakashima, E. F. Arcos, and M. Ortuzar, "Electric vehicle using a combination of ultracapacitors and ZEBRA battery," *IEEE Transactions on Industrial Electronics,* vol. 57, no. 3, pp. 943–949, Mar. 2010.

[12] Z. Amjadi and S. S. Williamson, "Power-electronics-based solutions for plug-in hybrid electric vehicle energy storage and management systems," *IEEE Transactions on Industrial Electronics,* vol. 57, no. 2, pp. 608–616, Feb. 2010.

[13] S. Bala, T. Tengnr, P. Rosenfeld, and F. Delince, "The effect of low frequency current ripple on the performance of a lithium iron phosphate LFP battery energy storage system," in 2012 *IEEE Energy Conversion Congress and Exposition (ECCE),* pp. 3485–3492, Sep. 2012.

[14] H. Z. Z. Beh, G. A. Covic, and J. T. Boys, "Effects of pulse and DC charging on lithium iron phosphate (LiFePO4) batteries," 2013 *Ieee Ecce*, pp. 315–320, 2013.

[15] S. Haghbin, S. Lundmark, M. Alakula, and O. Carlson, "Grid-connected integrated battery chargers in vehicle applications: Review and new solution," *IEEE Transactions on Industrial Electronics,* vol. 60, no. 2, pp. 459–473, Feb. 2013.

[16] K. M. S. Y. Konara and M. L. Kolhe, "Charging management of grid integrated battery for overcoming the intermittency of re sources," in 2016 *IEEE International Conference on Information and Automation for Sustainability (ICIAfS),* pp. 1–6, Dec. 2016.

[17] L. Shi, A. Meintz, and M. Ferdowsi, "Single-phase bidirectional AC-DC converters for plug-in hybrid electric vehicle applications*," in 2008 IEEE Vehicle Power and Propulsion Conference,* pp. 1–5, Sep. 2008.

[18] SAE Electric Vehicle and Plug-in Hybrid Electric Vehicle Conductive Charge Coupler, SAE Std. J1772, 2010.

[19] M. Grenier, M. G. H. Aghdam, and T. Thiringer, "Design of on-board charger for plugin hybrid electric vehicle*," in 5th IET International Conference on Power Electronics, Machines and Drives (PEMD 2010),* pp. 1–6, Apr. 2010.

[20] M. Yilmaz and P. T. Krein, "Review of battery charger topologies, charging power levels, and infrastructure for plug-in electric and hybrid vehicles," *IEEE Transactions on Power Electronics,* vol. 28, no. 5, pp. 2151–2169, May. 2013.

[21] O. C. Onar, J. Kobayashi, D. C. Erb, and A. Khaligh, "A bidirectional high-power quality grid interface with a novel bidirectional noninverted buck-boost converter for PHEVs," *IEEE Transactions on Vehicular Technology,* vol. 61, no. 5, pp. 2018–2032, Jun. 2012.

[22] J. C. Bendien, G. Fregien, and J. D. van Wyk, "High-efficiency on-board battery charger with transformer isolation, sinusoidal input current and maximum power factor,"*e*l. 1986.

[23] M. Pahlevaninezhad, P. Das, J. Drobnik, P. K. Jain, and A. Bakhshai, "A new control approach based on the differential flatness theory for an AC/DC converter used in electric vehicles*," IEEE Transactions on Power Electronics,* vol. 27, no. 4, pp. 2085– 2103, Apr. 2012.

[24] Y. J. Lee, A. Khaligh, and A. Emadi, "Advanced integrated bidirectional AC/DC and DC/DC converter for plug-in hybrid electric vehicles*," IEEE Transactions on Vehicular Technology,* vol. 58, no. 8, pp. 3970–3980, Oct. 2009.

[25] H. Chen, X. Wang, and A. Khaligh, "A single stage integrated bidirectional ac/dc and dc/dc converter for plug-in hybrid electric vehicles," in 2011 *IEEE Vehicle Power and Propulsion Conference,* pp. 1–6, Sep. 2011.

[26] Dusmez, Serkan and Khaligh, Alireza, "A novel low cost integrated on-board charger topology for electric vehicles and plug-in hybrid electric vehicles," *Conference Proceedings- IEEE Applied Power Electronics Conference and Exposition* - APEC, pp. 2611–2616, 2012.

[27] S. Dusmez and A. Khaligh, "A compact and integrated multifunctional power electronic interface for plug-in electric vehicles*," IEEE Transactions on Power Electronics,* vol. 28, no. 12, pp. 5690–5701, Dec. 2013.

[28] S. Dusmez and A. Khaligh, "A charge-nonlinear-carrier-controlled reduced-part single-stage integrated power electronics interface for automotive applications," *IEEE Transactions on Vehicular Technology,* vol. 63, no. 3, pp. 1091–1103, Mar. 2014.

[29] Y. Tang, D. Zhu, C. Jin, P. Wang, and F. Blaabjerg, "A three-level quasi-two-stage single-phase PFC converter with flexible output voltage and improved conversion efficiency," *IEEE Transactions on Power Electronics,* vol. 30, no. 2, pp. 717–726, Feb.2015.

[30] J. Perlin, Let it Shine*: The 6,000-Year Story of Solar Energy, New World Library,* 2013.

[31] K. Butti and J. Perlin, *Golden Thread: Twenty five hundred years of solar architecture and technology,* Cheshire Books, 1980.

[32] M. A. Green, "*The path to 25 % silicon solar cell* efficiency*: History of silicon cell evolution*," *Progress in Photovoltaics: Research and Applications*, vol. 17, no. 3, pp. 183-189, 2009.

[33] J. L. Loferski, "The first forty years: A brief history of the modern photovoltaic age," *Progress in Photovoltaics: Research and Applications*, vol. 1, no. 1, pp. 67-78, 1993.

[34] C. F. Gay and C. Eberspacher, "Worldwide photovoltaic market growth 1985-2000," *progress in photovoltaics: research and applications*, vol. 2, no. 3, pp. 249-255, 1994. \

[35] M. Green, "Silicon photovoltaic modules a brief history of the first 50 years," *Progress in Photovoltaics: Research and Applications*, vol. 13, no. 5, pp. 447-455, 2005.

[36] Snapshot of Global Photovoltaic Markets, International Energy Agency (IEA), 2015 [Online]. Available:http://www.iea-pvps.org/fileadmin/dam/public/report/PICS/IEA-PVPS_ __A_Snapshot_of_Global_PV_-_1992-2015_-_Final_2_02.pdf

[37] Bikash Kumar Sahu, "A study on global solar PV energy developments and policies with special focus on the top ten solar PV power-producing countries*," Renewable and Sustainable Energy Reviews*, vol. 43, pp. 621-634, March 2015.

[38] Ping Huang, Simona O. Negro, Marko P. Hekkert and Kexin Bi, "How China became a leader in solar PV: *An innovation system analysis," Renewable and Sustainable Energy Reviews*, vol. 64, pp. 777-789, October 2016.

[39] Physical Progress (Achievements), *Ministry of New & Renewable Energy, Govt. of India, 2016* [Online].

[40] Photovoltaics-*Historical development, PVRESOURCES, 2015* [Online]. Available: http://www.pvresources.com/en/introduction/history.php

[41] EnergyTrend-*PV, 11 October 2016* [Online].
Available: http://pv.energytrend.com/pricequotes.html

[42] U.S. Energy Information and Admiration*: Independent Statistics and Analysis 2019* [Online].
Available: https://www.eia.gov/tools/faqs/faq.php?id=19&t=3

[43] Quality Certification, Standards and Testing for Grid-connected rooftop solar PV systems/power plants, *ministry of new and renewable energy, Govt. of India, Feb. 2016* [Online]. Available: http://mnre.gov.in/file-manager/UserFiles/Rooftop-Solar-PV-Quality-Standards_Revised.pdf

[44] Draft Indian Standard, *Bureau of Indian Standards, 2014* [Online]. Available: http://www.bis.org.in/sf/etd/IEC-6756-59_23072014.pdf

[45] Indian Standard: Solar Photovoltaic Energy Systems—Terms, Definitions and Symbols, *Bureau of Indian Standards, June 2013.* [Online]. Available: https://law.resource.org/pub/in/bis/S05/is.12834.2013.pdf

[46] The overall efficiency of grid-connected photovoltaic inverters, *National Standards Authority of Ireland, 2010* [Online]. Available: https://infostore.saiglobal.com/store/

[47] Best Practice Regulation of the Australian Solar Industry, *Clean Energy Council, Feb. 2015* [Online]. Available: https://www.cleanenergycouncil.org.au/policyadvocacy/ reports.html

[48] Guide to Standards - *Solar Panels, SAI GLOBAL, Nov. 2011* [Online]. Available: http://infostore.saiglobal.com/store/

[49] J. Ahmed and Z. Salam, "A modified P&O maximum power point tracking method with reduced steady state oscillation and improved tracking efficiency," *IEEE Trans. Sustain. Energy,* vol. 7, no. 4, pp. 1506-1515, Oct. 2016.

[50] T. Andrejasic, M. Jankovec and M. Topic, "Comparison of direct maximum power point tracking algorithms using EN 50530 dynamic test procedure*," IET Renewable Power Generation,* vol. 5, no. 4, pp. 281-286, July 2011.

[51] M. A. Huque, S. J. Coley and T. S. Key, "Evaluating dynamic maximum power point tracking with variable solar irradiance," *IEEE 39th Photovoltaic Specialists Conference (PVSC), PART 2*, Tampa, FL, 2013, pp. 068-075.

[52] D. Sera, L. Mathe, T. Kerekes, S. V. Spataru and R. Teodorescu, "On the perturb-and-observe and incremental conductance MPPT methods for PV systems," *IEEE Journal of Photovoltaics*, vol. 3, no. 3, pp. 1070-1078, July 2013.

[53] B. Subudhi, and R. Pradhan, "A comparative study on maximum power point tracking techniques for photovoltaic power systems," *IEEE Transactions on Sustainable Energy,* vol.4, no.1, pp.89-98, Jan. 2013.

[54] M.A.G. de Brito, L. Galotto, L.P.Sampaio, G .e Melo de Azevedo and C.A. Canesin, "Evaluation of the main MPPT techniques for photovoltaic applications,"*IEEE Transactions on Industrial Electronics,* vol.60, no.3, pp.1156-1167, March 2013.

[55] Ali Reza Reisi, Mohammad Hassan Moradi and Shahriar Jamasb, "Classification and comparison of maximum power point tracking techniques for photovoltaic system: A review," *Renewable and Sustainable Energy Reviews,* vol. 19, pp. 433-443, March 2013.

[56] Boualem Bendib, Hocine Belmili, and Fateh Krim, "A survey of the most used MPPT methods: Conventional and advanced algorithms applied for photovoltaic systems," *Renewable and Sustainable Energy Reviews,* vol. 45, pp. 637-648, May 2015.

[57] Deepak Verma, Savita Nema, A.M. Shandilya, and Soubhagya K. Dash, "Maximum power point tracking (MPPT) techniques: Recapitulation in solar photovoltaic systems," *Renewable and Sustainable Energy Reviews,* vol. 54, pp. 1018-1034, February 2016.

[58] Hegazy Rezk and Ali M. Eltamaly, "A comprehensive comparison of different MPPT techniques for photovoltaic systems*," Solar Energy,* vol. 112, pp. 1-11, Feb. 2015.

[59] S. Jain and V. Agarwal, "Comparison of the performance of maximum power point tracking schemes applied to single-stage grid-connected photovoltaic systems*," IET Electric Power Applications,* vol. 1, no. 5, pp. 753-762, Sept. 2007.

[60] J.D. Bastidas-Rodriguez, E. Franco, G. Petrone, C. Andrés Ramos -Paja and G. Spagnuolo, "Maximum power point tracking architectures for photovoltaic systems in mismatching conditions: a review*," IET Power Electronics*, vol.7, no.6, pp.1396-1413, June 2014.

[61] Mohamed A. Eltawil and Zhengming Zhao, "MPPT techniques for photovoltaic applications," *Renewable and Sustainable Energy Reviews,* vol. 25, pp. 793-813, September 2013.

[62] Nabil Karami, Nazih Moubayed and Rachid Outbib, "General review and classification of different MPPT Techniques," *Renewable and Sustainable Energy Reviews,* vol. 68, Part 1, pp. 1-18, February 2017.

[63] Hadjer Bounechba, Aissa Bouzid, Hamza Snani, and Abderrazak Lashab, "Real-time simulation of MPPT algorithms for the PV energy system*," International Journal of Electrical Power & Energy Systems,* vol. 83, pp. 67-78, December 2016.

[64] Trishan Esram and Patrick L. Chapman, "Comparison of photovoltaic array maximum power point tracking techniques," *IEEE Trans. on Energy Conv.,* vol. 22, no. 2, June 2007.

[65] M. A. Elgendy, B. Zahawi, and D. J. Atkinson, "Operating characteristics of the P&O algorithm at high perturbation frequencies for standalone PV systems*," IEEE Trans. Energy Convers.,* vol. 30, no. 1, pp. 189-198, March 2015.

[66] M. Killi and S. Samanta, "Modified perturb and observe MPPT algorithm for drift avoidance in photovoltaic systems," *IEEE Trans. Ind. Electron.,* vol.62, no.9, pp.5549-5559, Sept. 2015.

[67] K. L. Lian, J. H. Jhang and I. S. Tian, "A maximum power point tracking method based on perturb-and-observe combined with particle swarm optimization," *IEEE Journal of Photovoltaics,* vol. 4, no. 2, pp. 626-633, March 2014.

[68] H. A. Sher, A. F. Murtaza, A. Noman, K. E. Addoweesh, K. Al-Haddad, and M. Chiaberge, "A new sensorless hybrid MPPT algorithm based on fractional short- circuit current measurement and P&O MPPT," *IEEE Trans. Sustain. Energy,* vol. 6, no. 4, pp. 1426-1434, Oct. 2015.

[69] K. Sundareswaran, V. Vigneshkumar, and S. Palani, "Development of a hybrid genetic algorithm/perturb and observe algorithm for maximum power point tracking in photovoltaic systems under non-uniform insolation," *IET Renewable Power Generation,* vol. 9, no. 7, pp. 757-765, Sept. 2015.

[70] G. J. Kish, J.J. Lee and P.W. Lehn, "Modelling and control of photovoltaic panels utilizing the incremental conductance method for maximum power point tracking," *IET Renewable Power Generation,* vol.6, no.4, pp.259-266, July 2012.

[71] M.A. Elgendy, B. Zahawi, and D.J. Atkinson, "assessment of the incremental conductance maximum power point tracking algorithm," *IEEE Trans. Sustain. Energy,* vol.4, no.1, pp.108-117, Jan. 2013.

[72] Zhou Xuesong, Song Daichun, Ma Youjie, and Cheng Deshu, "The simulation and design for mppt of pv system based on incremental conductance method," in *Proc. WASE International Conf. on Information Engineering (ICIE),* vol.2, 14-15 Aug. 2010, pp.314-317.

[73] Kok Soon Tey and S. Mekhilef, "Modified incremental conductance algorithm for photovoltaic system under partial shading conditions and load variation," *IEEE Trans. Ind. Electron.,* vol.61, no.10, pp.5384-5392, Oct. 2014.

[74] M. A. Elgendy, D. J. Atkinson and B. Zahawi, "Experimental investigation of the incremental conductance maximum power point tracking algorithm at high perturbation rates," *IET Renewable Power Generation,* vol. 10, no. 2, pp. 133-139, Feb. 2016.

[75] R. Faraji, A. Rouholamini, H.R. Naji, R. Fadaeinedjad and M.R. Chavoshian, "FPGA-based real-time incremental conductance maximum power point tracking controller for photovoltaic systems," *IET Power Electronics*, vol.7, no.5, pp.1294-1304, May 2014.

[76] P. Sivakumar, Abdullah Abdul Kader, Yogeshraj Kaliavaradhan and M. Arutchelvi, "Analysis and enhancement of PV efficiency with incremental conductance MPPT technique under non-linear loading conditions," *Renewable Energy*, vol. 81, pp. 543-550, September 2015.

[77] Abdelhamid Loukriz, Mourad Haddadi and Sabir Messalti, "Simulation and experimental design of a new advanced variable step size Incremental Conductance MPPT algorithm for PV systems," *ISA Transactions*, vol. 62, pp. 30-38, May 2016.

[78] N. E. Zakzouk, M. A. Elsaharty, A. K. Abdelsalam, A. A. Helal and B. W. Williams, "Improved performance low-cost incremental conductance PV MPPT technique," *IET Renewable Power Generation*, vol. 10, no. 4, pp. 561-574, Apr. 2016.

[79] D. C. Huynh and M. W. Dunnigan, "Development and Comparison of an improved incremental conductance algorithm for tracking the MPP of a solar PV panel," *IEEE Trans. Sustain. Energy*, vol. 7, no. 4, pp. 1421-1429, Oct. 2016.

[80] A. El Khateb, N. A. Rahim, J. Selvaraj, and M. N. Uddin, "Fuzzy-logic-controller- based SEPIC converter for maximum power point tracking," *IEEE Transactions on Industry Applications*, vol. 50, no. 4, pp. 2349-2358, July-Aug. 2014.

[81] Mohamed M. Algazar, Hamdy AL-monier, Hamdy Abd EL-halim, and Mohamed Ezzat El Kotb Salem, "Maximum power point tracking using fuzzy logic control," *International Journal of Electrical Power & Energy Systems*, vol. 39, no. 1, pp. 21-28, July 2012.

[82] F.A.O. Aashoor and F.V.P. Robinson, "Maximum power point tracking of photovoltaic water pumping system using fuzzy logic controller," in *Proc. 48th International Universities Power Engineering Conference*, 2-5 Sept. 2013, pp.1-5.

[83] A. A. S. Mohamed, A. Berzoy and O. Mohammed, "Design and hardware implementation of FL MPPT control for PV systems based on GA and small-signal analysis," *IEEE Transactions on Sustainable Energy*, vol. 8, no. 1, pp. 279-290, Jan. 2017.

[84] Y. Mahmoud and E. F. El-Saadany, "Fast power-peaks estimator for partially shaded PV systems," *IEEE Trans. Energy Convers*., vol. 31, no. 1, pp. 206-217, March 2016.

[85] E. Koutroulis and F. Blaabjerg, “A new technique for tracking the global maximum power point of PV arrays operating under partial-shading conditions*,” IEEE J. Photovoltaics, vol. 2*, no. 2, pp. 184–190, Apr. 2012.

[86] M. A. Ghasemi, H. Mohammadian Forushani, and M. Parniani, “Partial shading detection and smooth maximum power point tracking of PV arrays under PSC*,” IEEE Trans. Power Electron.*, vol. 31, no. 9, pp. 6281-6292, Sept. 2016.

[87] S. Mohanty, B. Subudhi and P. K. Ray, “A new MPPT design using grey wolf optimization technique for photovoltaic system under partial shading conditions*,” IEEE Transactions on Sustainable Energy*, vol. 7, no. 1, pp. 181-188, Jan. 2016.

[88] Y. Wang, Y. Li and X. Ruan, “High-accuracy and fast-speed MPPT methods for PV string under partially shaded conditions,” *IEEE Transactions on Industrial Electronics*, vol. 63, no. 1, pp. 235-245, Jan. 2016.

[89] R. Kotti and W. Shireen, “Efficient MPPT control for PV systems adaptive to fast-changing irradiation and partial shading conditions,” *Solar Energy*, vol. 114, pp. 397– 407, Mar. 2015.

APPENDIX-A

SIMULATION SETUP

This appendix explains about more detail of simulation setup that have been conducted in order to investigate the performance of the proposed converters in each mode of vehicle operation.

The simulations were conducted in MATLAB/Simulink environment. MATLAB is widely used as an interactive tool for modelling, analysis and visualization of systems, which itself contains more than 600 mathematical functions and supports additional toolboxes to make it more comprehensive. Simulink is a MATLAB add-on software that enables block diagram-based modelling and analysis of linear, nonlinear, discrete, and continuous and hybrid systems. The power circuit of the proposed topologies has been modelled using Sim Power- Systems toolbox of 2013a MATLAB version. The control circuit has been developed using 'Math Operations', 'Signal Routing, 'Discrete', 'Sink' and 'Source' blocks of Simulink. The simulation sample time has been kept $1e^{-6}$ s for the execution of power circuit.

APPENDIX-B
SPECIFICATIONS OF PV MODULE HB-40

The complete specifications of an HBL Power systems Ltd. make PV module HB-40 are given below. All electrical parameters are measured at STC (25°C, 1000 W/m^2, 1.5 AM). This module is used to design a PV array in Chapter 3.

Electrical Specifications:

Numbers of cells in a module	36
Maximum Power	40 W
Open circuit voltage	21 V
Short circuit current	2.27 A
Voltage at MPP	18.86 V
Current at MPP	2.12 A

Mechanical Specifications:

Size - L×W×T	655×480×34
Weight	4.15 kg

Thesis 5

ORIGINALITY REPORT

15%	6%	13%	%
SIMILARITY INDEX	INTERNET SOURCES	PUBLICATIONS	STUDENT PAPERS

PRIMARY SOURCES

1	Ankit Kumar Singh, Mukesh Kumar Pathak. "A Multi-Functional Single-Stage Power Electronic Interface for Plug-In Electric Vehicles Application", Electric Power Components and Systems, 2018 Publication	2%
2	Ankit Kumar Singh, Mukesh Kumar Pathak. "Integrated converter for plug-in electric vehicles with reduced sensor requirement", IET Electrical Systems in Transportation, 2019 Publication	2%
3	www.iejrd.com Internet Source	1%
4	Ankit Kumar Singh, Mukesh Kumar Pathak. "A Comprehensive Review of Integrated Charger for on-Board Battery Charging Applications of Electric Vehicles", 2018 IEEE 8th Power India International Conference (PIICON), 2018 Publication	1%
5	Ankit Kumar Singh, Anjanee Kumar Mishra, Krishna Kumar Gupta, Pallavee Bhatnagar,	1%